INFORMATION TO USERS

This manuscript has been reproduced from the microfilm master. UMI films the text directly from the original or copy submitted. Thus, some thesis and dissertation copies are in typewriter face, while others may be from any type of computer printer.

The quality of this reproduction is dependent upon the quality of the copy submitted. Broken or indistinct print, colored or poor quality illustrations and photographs, print bleedthrough, substandard margins, and improper alignment can adversely affect reproduction.

In the unlikely event that the author did not send UMI a complete manuscript and there are missing pages, these will be noted. Also, if unauthorized copyright material had to be removed, a note will indicate the deletion.

Oversize materials (e.g., maps, drawings, charts) are reproduced by sectioning the original, beginning at the upper left-hand corner and continuing from left to right in equal sections with small overlaps.

Photographs included in the original manuscript have been reproduced xerographically in this copy. Higher quality 6" x 9" black and white photographic prints are available for any photographs or illustrations appearing in this copy for an additional charge. Contact UMI directly to order.

ProQuest Information and Learning
300 North Zeeb Road, Ann Arbor, MI 48106-1346 USA
800-521-0600

UNIVERSITÉ DE SHERBROOKE
Faculté de Génie
Département de Génie Mécanique

PRÉVISION DE LA RUPTURE DES COMPOSITES POLYESTER/ TISSUS DE VERRE

PREDICTION OF FAILURE IN POLYESTER REINFORCED BY WOVEN GLASS FABRICS

Mémoire de maîtrise ès sciences appliquées
Spécialité : Génie Mécanique

Hoi Nguyen-Hoa

Sherbrooke (Québec), CANADA Mai 1999

SOMMAIRE

Les matériaux composites sont de nos jours de plus en plus utilisés dans différents domaines soit : l'aéronautique, les équipements de sport et le domaine militaire. La popularité du matériau s'explique par ses bonnes propriétés mécaniques. De plus, on peut modéliser à volonté les propriétés de la structure composite selon les exigences de la conception. En particulier, les fibres tissées sont la forme la plus utilisée dans les applications structurales. Leurs propriétés mécaniques intéressantes, leur facilité d'utilisation et leur bonne capacité de déformation donnent aux composites une grande attraction pour la fabrication des formes complexes.

Cependant, l'un des principaux problèmes concernant les composites est le cycle de fabrication. En effet, lors du moulage des matériaux composites stratifiés, les fibres sont très fortement réorientées afin de se conformer à la géométrie du moule. Après la déformation, le composite tissé devient une structure non-orthogonale. Alors, les trois modèles principaux bien connus : le modèle à mosaïque, le modèle à ondulation et le modèle à pont; ne sont pas appropriés pour prédire les comportements thermo-élastiques ainsi que la rupture du composite tissé. Un autre modèle appelé « le modèle à sous-plis » qui a été proposé par D. Laroche et T. Vu-Khanh [28-29] a surmonté ce défaut.

La prédiction de la rupture des matériaux composites renforcés de fibres tissées constitue l'objectif principal de ce projet. Le problème vise donc à appliquer le modèle à sous-

plis et des critères de rupture pour prédire les résistances des composites tissés déformés. Pour considérer l'effet d'ondulation des fibres, deux types de fibres tissées sont utilisés : la toile et le satin-8. Les composites sont faits de polyester et de fibre de verre avec une fraction volumique de fibres d'environ 48-52%.

Pour faire la prédiction de la rupture des composites tissés à l'aide du modèle à sous-plis, il faut d'abord exécuter des tests en traction sur des échantillons à fibres orthogonaux, $[(0/90)_n]_s$, et non-orthogonaux avec $\theta = 45^0$, $[(\pm 45)_n]_s$, en composites tissés. De ces résultats expérimentaux, nous pouvons déterminer les propriétés mécaniques de ces composites tissés. Particulièrement, une approche pour déterminer les coefficients de la résistance qui inclut l'effet d'ondulation des fibres a été proposée. Les résistances prédites en tension et en compression sont déterminées par l'utilisation d'une procédure de plis dégradés proposée dans [47]. Ensuite, des tests, qui mesurent les résistances, sont effectués pour vérifier la validité des prédictions de deux critères de rupture soit le critère quadratique et le critère de la déformation maximale. Finalement, une observation microscopique est réalisée pour expliquer les phénomènes d'endommagement des composites tissés.

Les résultats prédits sont conformes aux données expérimentales. Les prédictions théoriques obtenues à l'aide du modèle à sous-plis et du critère quadratique confirment avec beaucoup plus de succès les mesures expérimentales que les prédictions données par le critère de la déformation maximale. C'est la raison pour laquelle seul le critère quadratique a été présenté.

ABSTRACT

Polyester/glass fiber is probably by far the most commonly used composite. This work presents the results of an investigation on the failure of plain weave and 8-harness satin glass/polyester composites. The emphasis is put on the prediction of the failure envelopes in these materials. It is well known that the forming process of fabric composites usually results in significant in-plane shear deformations of the interlaced yarns and the reinforcement fabric becomes a non-orthogonal structure. It is therefore important to be able to predict the mechanical properties of woven fabric composites as a function of shear deformation of the interlaced yarns. To predict the failure strengths of any deformed fabric composites, the sub-plies model was used. In this model, woven fabric composites are divided into four fictional unidirectional sub-plies with orthotropic properties that are laid up in an unsymmetrical configuration. Consequently, the strength of woven fabric laminate is predicted as a function of the failure parameters of the constituent sub-plies and the in-plane shearing deformation angle between these plies. Another major advantage of the model is that it allows the direct use of laminated shell element in finite element codes for structural analysis. In order to take account of fiber undulation effect on mechanical properties, a procedure for the determination of the equivalent on-axis tensile and compressive strength coefficients of the constituent plies is also proposed. In this procedure, the material coefficients of the constituents plies were determined by measuring the mechanical properties of $[(0/90)_n]_s$ and $[(-45/45)_n]_s$ specimens

made of the woven fabric composite. To verify the theoretical prediction, the tensile and compressive tests were carried out at room temperature on the specimens. The tests were performed according to procedure recommended standards by ASTM D-3039 and ASTM D-3410 (Celanese compression test fixture). Before moulding the interlaced yarns of the fabric structure in the moulded samples were deformed by shearing to various angles.

The maximum strain and quadratic criteria were used to predict the failure envelope of the composites. The onset of damage was compared with prediction from the first ply failure of the sub-plies model. The predicted ultimate strength was determined using the procedure proposed in [47] to simulate the gradual degradation of the laminate due to the failure of successive plies with increasing loading. The predicted results are in good agreement with the experimental data. Prediction, using the sub-plies model and the quadratic criterion, is found to be in better agreement with experimental measurements than that using the sub-plies model and the maximum strain criterion so that only predictions from the quadratic criterion are presented. Deformation and failure behavior in woven fabric composites are also presented, specially, the observed evolution of damage in woven composite under uniaxial tensile and compressive loading conditions.

PREFACE

My research described in this dissertation was carried out in the Mechanical Engineering Department, Faculté de génie, Université de Sherbrooke.

I am very grateful to my supervisor Mr Toan Vu-Khanh for his help, support, kind advice and encouragement through the nearly two years research. Thanks must also be given to Mr Magella Tremblay for assistance with the experimental work and to many other members of the "Polymers and Composites Group" and the Mechanical Engineering Department, in particular the workshops personnel, the library staff, etc.

Finally, I am extremely grateful to my parent, brothers and sisters for their loves, supports and encouragement.

This dissertation is the result of my own work and includes nothing, which is the outcome of work done in collaboration. A part of this dissertation has been presented at Japan-Canada conference on last August 1998 and sent to the Journal of Composite Materials for publication.

May, 1999 Hoi Nguyen-Hoa

TABLE OF CONTENTS

LIST OF FIGURES

LIST OF TABLES

LIST OF SYMBOLS

$\overline{A_{ij}}$, $\overline{B_{ij}}$ and $\overline{D_{ij}}$: the rigid coefficients

$\overline{M_i}$: average moments

$\overline{N_i}$: average stresses

σ_1, σ_2, σ_6 : stress components in the reference coordinate axes.

ε_S : maximum allowable shear strain in x-y plane.

σ_x, σ_y, σ_s : stress components in the material symmetry axes.

ε_{Xt} (ε_{Xc}) : maximum allowable tension (compressive) normal strain in the x-direction.

ε_{Yt} (ε_{Yc}) : maximum allowable tension (compressive) normal strain in the y-direction.

2θ : deformation angle between the warp and weft threads.

C_i : the constants are evaluated similar to Hill' s criterion.

E_S : longitudinal shear modulus.

E_x : longitudinal Young' s modulus.

E_y : transversal Young' s modulus.

F_{ij}, F_i : strength parameters in stress space: i,j = x, y, z.

h : a thickness of fabric.

k : the k-th layer.

N : total numbers of ply (or layer)

$n_g a$: a unit of length

S (%) : the region of damage zone.

S : shear strength coefficient in the (x-y) plane (the failure stress in pure shear).

S_4, S_5 : transverse shear strengths.

X, (X') : tensile (compressive) strength coefficient in the x direction;

x, y are the principal material directions;

X_f : ultimate strength of fiber.

X_m, Y_m and S_m : ultimate strengths of matrix.

Y, (Y') : tensile (compressive) strength coefficient in the y direction;

z : position of ply in z-direction.

Chapter 1

INTRODUCTION

In the past thirty to thirty-five years, intensive effort has gone into the research and development of composite materials even though the concept of using two or more distinct materials combined to form the constituent phases of a composite material has been practiced ever since materials were first used. One of these constituents forms a continuous phase and called the matrix. The other major constituent is reinforcement in the form of fibers or particulates that are, in general, added to the matrix to improve or alter the matrix properties. The development of fiber reinforced composite materials recently has led to their use in many advanced structures due to the inherent high strength, low weight, and specific electrical, acoustic and magnetic properties, and also their ability to be tailored made to meet complex shape and strength problems.

Many advanced fiber composites can be produced that have the same strength and stiffness as the strongest steels, yet are seventy percent lighter [24]. Others can be made for aircraft that are three times stronger than aluminum alloys, yet are forty percent lighter.

Composite materials are also being used more and more in conventional ground transportation when their use is cost competitive. Their use would cut down vehicle weight considerably, thereby improving fuel efficiency. Polymer matrix composites are presently

being developed to take the place of metals in applications such as body panels, drive shafts, entire truck frames, brake systems and engine blocks.

Fiber composites are presently being used quite successfully in the recreational arena for improved performance and weight reduction without compromising strength. Such applications include golf club shafts, tennis rackets, canoes, boat bodies and skis and the list is continually growing.

In terms of matrix material, the most common resin used in composites is unsaturated polyester [48]. This is due to lower cost of the resin and also its adaptability to fabrication of large structures. Among the three common reinforcing fibers: glass, carbon, and aramid, glass is by the far the most popular in terms of volume consumption. This is due to the lower cost and respectable performances offered. However, the matrix and fibers should be selected according to performance required and cost effectiveness.

There are many different types of reinforced glass fiber and the portion of reinforcement to matrix may be altered to meet any specific application. Woven fabrics are now considered to be a more important reinforcing material in the composite technology than a decade ago. Although the structure efficiency of fabric composites is not as high as that of the unidirectional laminates, their handling properties and low fabrication costs have made fabric composites attractive for structural applications [34]. Most woven fabrics are essentially two-dimensional and consist of two sets of yarns interlaced at a 90° angle. The various types of fabric structures can be identified by the pattern of their repeating regions. They are characterized by a geometrical parameter, n_g, that denotes that a warp thread is interlaced with every n_g-*th* fill thread [7-8,19-22]. The most common patterns of woven fabrics are plain

weave (n_g = 2), twill weave (n_g = 3), crowfoot satin or 4-harness satin (n_g = 4), 5-harness satin (n_g = 5) and 8-harness satin (n_g = 8). Figure 1.1 shows some examples of woven fabric patterns.

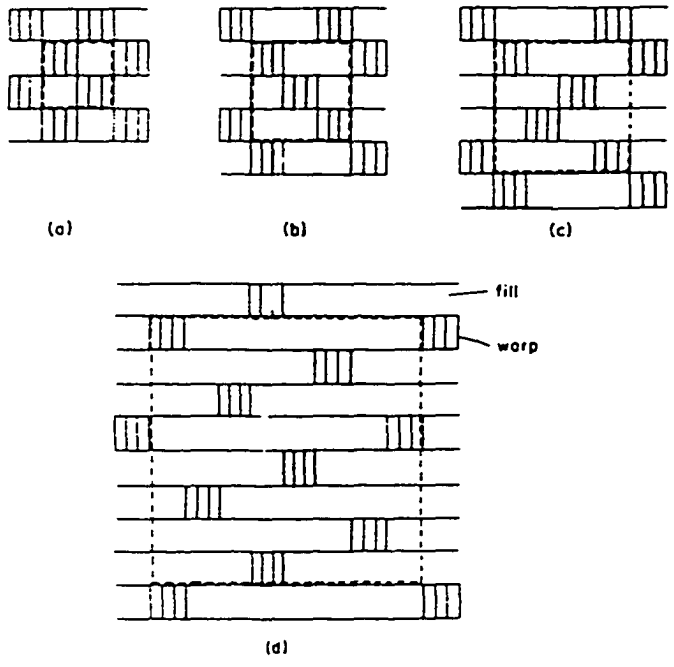

Figure 1.1 : Examples of woven fabric patterns : (a) plain weave (n_g = 2); (b) twill weave (n_g = 3); (c) 4-harness satin (n_g = 4); (d) 8-harness satin (n_g = 8).

In order to predict the macroscopic behavior of woven fabric composites, recent studies have focused on the development of micro-mechanical models that can be applied to various fabric structures (various values of n_g). The three current models are known as the mosaic model, the crimp model, and the bridging model.

When the part has a double curvature, the forming process usually results in significant in-plane shear deformation of the interlaced yarns and the fabric composite becomes a non-

orthogonal structure (Figure 1.2), so these models can no longer be valid. Furthermore, the failure process in these materials is relatively complex and only a few studies have been reported on the prediction of strength for orthotropic woven fabric composites [37,43]. The lack of analysis tools is therefore a major obstacle in design and structural analysis of these materials.

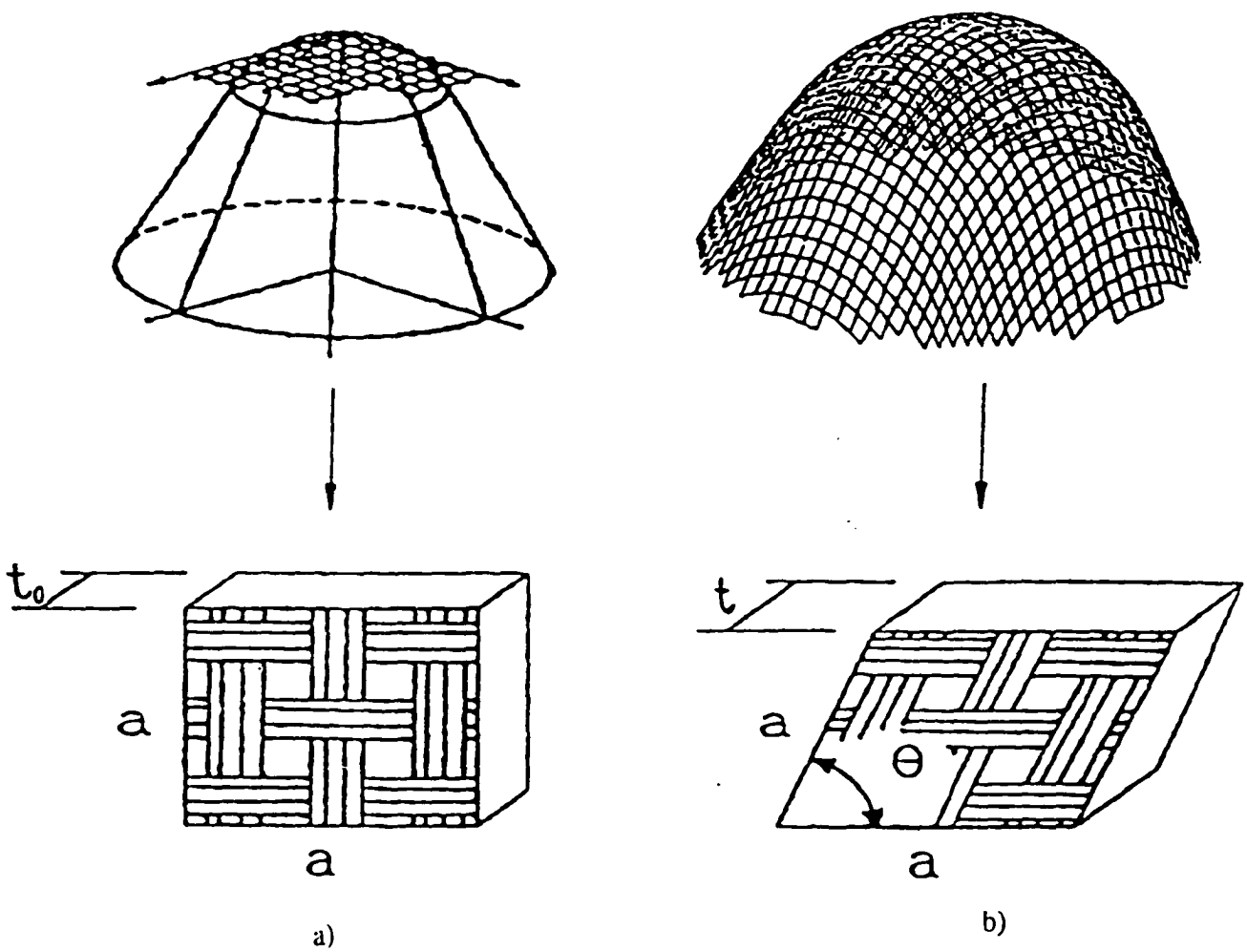

Figure 1.2 : Deformation of an orthogonal fabric after draping a rounded top cone :

(a) orthogonal fabric structure; (b) deformed fabric structure

Recently, a sub-plies model has been proposed for the characterization of the thermo-elastic properties for any deformed woven fabric composite [28-29,50-52]. This work aims at applying the sub-plies model in the prediction of tensile and compressive strengths of orthogonal and non-orthogonal woven fabric laminates. The effect of fiber undulation and yarns' interlacing on failure behavior are analyzed. A special method is proposed to determine the equivalent on-axis strength coefficients of the constituent sub-plies. The ultimate strength and the onset of damage as a function of the in-plane shearing deformation angle were analyzed.

Chapter 2

LITERATURE REVIEW

2.1. FAILURE THEORIES FOR COMPOSITE MATERIALS

2.1.1. Introduction

When using a material for a particular application, the design must be functional, both in design and efficiency. In some stage of the design, a comparison must be made between the state of stress existing in the material to a failure or strength criterion for that material. These criteria are usually expressed in terms of stress or sometimes strain. They can refer to the complete rupture or to some initial event such as cracking or yielding that would eventually lead to the total failure. Even though failure criteria are also widely interpreted, they have met with reasonable success in most isotropic materials. However, when these criteria are applied to anisotropic materials, in most cases, considerable error is evident between predicted and experimental data even when the criteria have been generalized or modified. The greatest error seems to be in cases where the material is non-homogeneous in nature, and fiber composites obviously belong to this category. This is because the production of free surfaces during crack propagation can only occur in the matrix, fiber, or the interface between the two. The homogeneous anisotropic elasticity theory, when applied to homogeneous materials, assumes that the crack extends into a material with the combined properties of the fiber and matrix. It is

well established that the properties of an orthotropic or anisotropic material change as the coordinate system is rotated, i. e., they are orientation dependant. Usually, the stresses are written with respect to the principal material directions and designated as σ_x, σ_y, ..., σ_s in contracted notation. In plane stress, the stresses associated with the x, y axes are normal stresses σ_x and σ_y and the in-plane shear stress σ_s (σ_{xy}), the other stress components being equal to zero. A general plane stress state σ_x, σ_y, σ_s is obtained whenever normal stresses σ_1, σ_2 are applied to a material, except for the one situation where these normal stresses coincide with the principal material direction, i. e., $\sigma_x = \sigma_1$, $\sigma_y = \sigma_2$ and the in-plane shear stress $\sigma_{xy} = 0$.

There are many different ways of classifying failure theories. One can, for example, classify them with respect to their stress interactivity or non-interactivity. In this context, the maximum stress or maximum strain theories would be considered non-interactive, whereas the Hill criterion is an interactive one.

A failure criterion describes the failure envelope of a lamina which is generally one layer of a composite material called laminate. In order to obtain the failure envelope of a laminated composite, we would have to superimpose the envelopes described by each ply (lamina) of the laminate. Care is therefore required because normal and shear stresses can be induced by lamina interactions and the actual lamina stresses must be analytically determined.

The strength of laminated anisotropic composites is dependent on the thermo-mechanical properties of the constituents layers and on the method of lamination which includes the thickness and orientation of layer, the stacking sequence, cross-ply ratio, helical angle, the laminating temperature, etc.

Strength tests on off-axis and angle-ply laminates offer useful information for the evaluation of the failure theory and failure mechanism. A number of failure criteria have been proposed to predict the failure of anisotropic composite materials under various states of stress.

2.1.2. Maximum stress theory

In the maximum stress theory, failure is said to occur when the stresses in the principal material directions exceed their respective strengths. Therefore, for no failure to occur in tension :

$$\begin{aligned} \sigma_x &< X \\ \sigma_y &< Y \\ |\sigma_s| &< S \end{aligned} \qquad (2.1.)$$

and for compression,

$$\begin{aligned} \sigma_x &> X' \\ \sigma_y &> Y' \end{aligned}$$

where :

x, y : the principal material directions;

X, (X') : tensile (compressive) strength in the 1 direction;

Y, (Y') : tensile (compressive) strength in the 2 direction;

S : shear strength in the (x-y) plane (the failure stress in pure shear).

If one or more of the above inequalities is not satisfied, it is assumed that failure has occurred. Note that there is no interaction between strengths or failure modes in this criterion.

Actually, there are three independent criteria in one. When $\sigma_s = 0$ and $X = X' = Y = Y'$, the geometric representation is a square with its center coincident with the origin of the reference axes.

On order to apply this criterion to a design, the stresses must be transformed into the principal material directions. So, for a unidirectional composite in a uniaxially loaded state at any angle θ from the fibers (Figure 2.1).

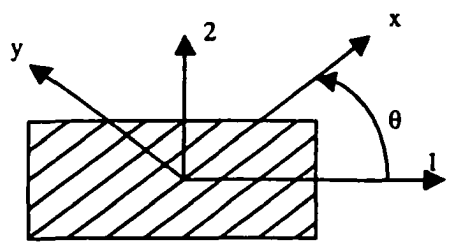

Figure 2.1 : Principal material coordinates of a lamina

For the simple case of uniaxial tensile loading with only σ_1 present and $\sigma_2 = \sigma_{12} = 0$, the stresses in the principal material directions are :

$$\sigma_x = \sigma_1 \cos^2\theta$$

$$\sigma_y = \sigma_1 \sin^2\theta \qquad (2.2.)$$

$$\sigma_s = -\sigma_1 \sin\theta \cos\theta$$

By substituting in the material strengths and solving for σ_1, failure does not occur as long as :

$$\sigma_1 < \frac{X}{\cos^2\theta}$$

$$\sigma_1 < \frac{Y}{\sin^2\theta} \qquad (2.3.)$$

$$\sigma_1 < \frac{S}{\sin\theta \cos\theta}$$

Following this criterion, the predicted uniaxial strength for E glass/epoxy composite is plotted in Figure 2.2 versus the angle θ between the loading direction and the principal material directions.

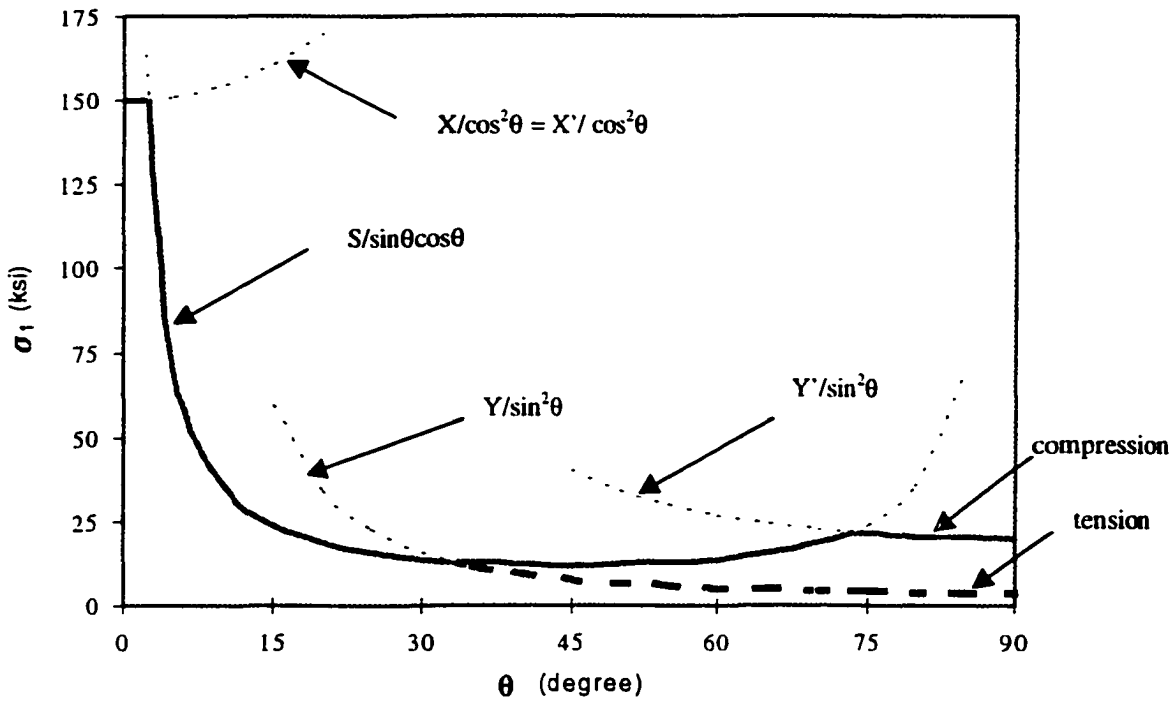

Figure 2.2 : The maximum stress failure criterion showing no interaction between failure mechanisms (reproduced from Ref. [24])

The tension data are denoted by solid circles and the compression data by solid squares. The maximum stress theory is shown as several solid curves, the lowest one of which governs the strength.

2.1.3. Maximum strain criterion

The maximum strain criterion is very similar to the maximum stress criterion. In this theory, failure will result if one or more of the following inequalities is not satisfied :

$$\varepsilon_x < \varepsilon_{Xt}$$

$$\varepsilon_y < \varepsilon_{Yt} \qquad (2.4.)$$

$$|\varepsilon_s| < \varepsilon_S$$

for tension and for compression :

$$\varepsilon_x > \varepsilon_{Xc}$$

$$\varepsilon_y > \varepsilon_{Yc}$$

where :

x, y : the principal material directions.

ε_{Xt} (ε_{Xc}) : maximum allowable tension (compressive) normal strain in the x-direction.

ε_{Yt} (ε_{Yc}) : maximum allowable tension (compressive) normal strain in the y-direction.

ε_S : maximum allowable shear strain in x-y plane.

As with the maximum stress theory, the strain in the material must be transformed to the principal material axes before the criterion can be applied. For the simple case of uniaxial tensile loading with only σ_1 presents and $\sigma_2 = \sigma_{12} = 0$, first, the stress transformation equation :

$$\sigma_x = \sigma_1 \cos^2\theta$$

$$\sigma_y = \sigma_1 \sin^2\theta \qquad (2.5.)$$

$$\sigma_s = -\sigma_1 \sin\theta \cos\theta$$

must be substituted into the stress-strain relations :

$$\varepsilon_x = \frac{1}{E_x}(\sigma_x - \nu_{xy}\sigma_y)$$
$$\varepsilon_y = \frac{1}{E_y}(\sigma_y - \nu_{yx}\sigma_x) \qquad (2.6.)$$
$$\varepsilon_s = \frac{\sigma_s}{E_s}$$

to get :

$$\varepsilon_x = \frac{1}{E_x}(\cos^2\theta - \nu_{xy}\sin^2\theta)\sigma_1$$
$$\varepsilon_y = \frac{1}{E_y}(\sin^2\theta - \nu_{yx}\cos^2\theta)\sigma_1 \qquad (2.7.)$$
$$\varepsilon_s = \frac{-1}{E_s}(\cos\theta\sin\theta)\sigma_1$$

Now, assuming the usual restrictions of linear elastic behavior to failure :

$$\varepsilon_{Xt} = \frac{X}{E_x}$$
$$\varepsilon_{Yt} = \frac{Y}{E_y} \qquad (2.8.)$$
$$\varepsilon_S = \frac{S}{E_s}$$

Finally, the maximum strain criterion can be expressed as :

$$\sigma_1 < \frac{X}{\cos^2\theta - \nu_{xy}\sin^2\theta}$$
$$\sigma_1 < \frac{Y}{\sin^2\theta - \nu_{xy}\cos^2\theta} \qquad (2.9.)$$
$$\sigma_1 < \frac{S}{\cos\theta\sin\theta}$$

From these equations, it can be seen that the only difference between the maximum stress and maximum strain theories is the inclusion of the Poisson terms in the latter. The plot of strength against fiber angle is very similar to the maximum stress theory. Again, this theory allows no interaction between stresses.

2.1.4. Interaction criteria

The Tsai-Hill theory, initially proposed by Hill [17], is actually a Von Mises' isotropic criterion extended into the realm of anisotropy. This criterion follows experimental data much better than either the maximum stress or strain theories and is defined as follows :

$$(G+H)\sigma_x^2+(F+H)\sigma_y^2+(F+G)\sigma_z^2-2H\sigma_x\sigma_y-2G\sigma_y\sigma_z-2F\sigma_z\sigma_y+ 2L\sigma_{zy}^2+2M\sigma_{xz}^2+2N\sigma_{xy}^2=1 \qquad (2.10.)$$

This is actually a yielding criterion but can be thought of a strength criterion since both yielding and strength can be considered as limits of linear elastic behavior. The coefficients F, G, H, L, M and N in the above equation are parameters characteristic of the state of anisotropy and are sometimes loosely called failure strength parameters.

Tsai related the failure strength parameters to the usual failure strengths X, Y, Z and S as follows. If only a shear stress, σ_{xy}, acts on the body, then :

$$2N=\frac{1}{S^2} \qquad (2.11.)$$

Similarly, if only a normal stress, σ_1, acts on the body then :

$$G + H = \frac{1}{X^2} \tag{2.12.}$$

Likewise, if only σ_2 acts on the body then :

$$F + H = \frac{1}{Y^2} \tag{2.13.}$$

If only a stress, σ_3, in a thickness direction acts on the body, and Z denotes the strength in the 3-direction, then :

$$F + G = \frac{1}{Z^2} \tag{2.14.}$$

Combining the latter three equations results in :

$$\begin{aligned} 2H &= \frac{1}{X^2} + \frac{1}{Y^2} - \frac{1}{Z^2} \\ 2H &= \frac{1}{X^2} - \frac{1}{Y^2} + \frac{1}{Z^2} \\ 2H &= -\frac{1}{X^2} + \frac{1}{Y^2} + \frac{1}{Z^2} \end{aligned} \tag{2.15.}$$

When plane stress is assumed, the constants L and M vanish, and we obtain the following condition :

$$\frac{\sigma_x^2}{X^2} - \sigma_x \sigma_y \left(\frac{1}{X^2} + \frac{1}{Y^2} + \frac{1}{Z^2} \right) + \frac{\sigma_y^2}{Y^2} + \frac{\sigma_{xy}^2}{S^2} = 1 \tag{2.16.}$$

If a unidirectional composite is considered to be in a state of plane stress (x-y plane) with the fibers oriented in the x-direction, then all stresses associated with the thickness direction are zero : σ_s (σ_{xy}) = σ_{xz} = σ_{yz} = 0. Note also that the y and z-directions are identical, both being

transverse directions, so Y = Z. Therefore, for a plane stress case, the Tsai-Hill equation (Eq.2.10) reduces to :

$$\frac{\sigma_x^2}{X^2} - \frac{\sigma_x \sigma_y}{X^2} + \frac{\sigma_y^2}{Y^2} + \frac{\sigma_{xy}^2}{S^2} = 1 \qquad (2.17.)$$

If a unidirectional composite is considered with the fibers oriented at any off axis angle θ, then the transformation equations for uniaxial loading (2.5.), can be substituted into the above equation to give :

$$\frac{\cos^4\theta}{X^2} + \left(\frac{1}{S^2} - \frac{1}{X^2}\right)\cos^2\theta \sin^2\theta + \frac{\sin^4\theta}{Y^2} = \frac{1}{\sigma_1^{\,2}} \qquad (2.18.)$$

A typical plot of strength versus ply-angle will be shown later when this criterion is applied to experimental data. The Tsai-Hill theory yields a smooth single curve instead of a three-part curve like the maximum stress and strain theories. The curve shows a continuous decrease in strength as θ goes from 0 to 90 degrees, sometimes with a little hump depending on the relative values of X, Y, and S, which in fact fits experimental data fairly well. This criterion also allows considerable interaction between failure stresses unlike the previous two criteria.

The Norris interaction theory [38] is empirical and was postulated to fit experimental data from plywood and orthotropic materials. The criterion is similar to the distortion energy type, except there is no cross-term in σ_x, σ_y :

$$\frac{\sigma_x^2}{X^2} + \frac{\sigma_y^2}{Y^2} + \frac{\sigma_s^2}{S^2} = 1 \qquad (2.19.)$$

Fisher [12] attempted to extend the Norris failure theory to predict of any laminate layer by introducing a constant derived from elastic modulus into the σ_x - σ_y cross term. However, by using elastic constants, linear elasticity is implied which is seldom the case in composites. The modified condition can be written as :

$$\frac{\sigma_x^2}{X^2} - \kappa\frac{\sigma_x\sigma_y}{XY} + \frac{\sigma_y^2}{Y^2} + \frac{\sigma_{xy}^2}{S^2} = 1 \qquad (2.20.)$$

where κ is given by :

$$\kappa = \frac{E_x(1+\nu_{yx}) + E_y(1+\nu_{xy})}{2\left[E_xE_y(1+\nu_{yx})(1+\nu_{xy})\right]^{1/2}} \qquad (2.21.)$$

Hoffman [18] extended Hill's theory to account for differences in tensile and compressive strengths by introducing linear terms in σ_x, σ_y and σ_{xy} into Hill's equation.

$$C_1(\sigma_y - \sigma_z)^2 + C_2(\sigma_z - \sigma_x)^2 + C_3(\sigma_x\sigma_y) + C_4\sigma_x + C_5\sigma_y + C_6\sigma_z + C_7\sigma_{zy}^2 + C_8\sigma_{xz}^2 + C_9\sigma_{xy}^2 = 1 \qquad (2.22.)$$

where the constants C_i are evaluated similar to Hill.

$$C_1 = \frac{1}{2}\left(\frac{1}{YY'} + \frac{1}{ZZ'} - \frac{1}{XX'}\right)$$

$$C_2 = \frac{1}{2}\left(\frac{1}{XX'} + \frac{1}{ZZ'} - \frac{1}{YY'}\right)$$

$$C_3 = \frac{1}{2}\left(\frac{1}{YY'} + \frac{1}{XX'} - \frac{1}{ZZ'}\right)$$

$$C_4 = \frac{1}{X} - \frac{1}{X'}$$

$$C_5 = \frac{1}{Y} - \frac{1}{Y'} \qquad (2.23.)$$

$$C_6 = \frac{1}{Z} - \frac{1}{Z'}$$

$$C_7 = \frac{1}{S_4^2}$$

$$C_8 = \frac{1}{S_5^2}$$

$$C_9 = \frac{1}{S^2}$$

where S_4 and S_5 are transverse shear strengths.

For plane stress conditions, assuming transverse isotropy with respect to the x-direction, equation above reduces to :

$$\frac{\sigma_x^2 - \sigma_x\sigma_y}{XX'} + \frac{\sigma_y^2}{YY'} + \frac{X - X'}{XX'}\sigma_x + \frac{Y' - Y}{YY'}\sigma_y + \frac{\sigma_{xy}^2}{S^2} = 1 \qquad (2.24.)$$

There is no physical significance attached to this failure condition.

Marin [31] proposed a distortion energy condition for orthotropic materials, but this is limited to when principal stresses σ_x and σ_y coincide with the principal stresses. The condition can be written as :

$$\frac{\sigma_x^2 + \sigma_y^2}{XX'} + \left(\frac{1}{X} - \frac{1}{X'}\right)\sigma_x + \left(\frac{1}{Y} - \frac{Y}{XX'}\right)\sigma_y + \left[\frac{2}{XX'} - \frac{1}{S^2} + \frac{1}{S}\left(\frac{1}{X} - \frac{1}{X'} - \frac{1}{Y} + \frac{1}{XX'}\right)\right]\sigma_x\sigma_y \geq 1 \qquad (2.25.)$$

Franklin [13] modified Marin' s theory to include a constant K_2 whose determination was directly dependent upon experimental complex stress data :

$$\frac{\sigma_x^2 - K_2\sigma_x\sigma_y}{XX'} + \frac{\sigma_y^2}{YY'} + \frac{Y' - Y}{YY'}\sigma_x + \frac{Y' + Y}{YY'}\sigma_y + \frac{\sigma_{xy}^2}{S^2} = 1 \qquad (2.26.)$$

The equation above can be rearranged to provide a K_2 value. By determining K_2 values for each quadrant, the failure envelope is forced to pass through the data used to determine it, and hence, a curve-fitting parameter is introduced to obtained better correlation between experimental and predicted values.

2.1.5. Strength tensor criteria

The concept of a strength tensor analogous to that for elastic constants was introduced by Kopnov [15], Ashkenazi [2] and later by Tsai and Wu [46]. These criteria are mainly the failure criteria for generally anisotropic materials and could account for differences in tensile compressive strengths and the dependence of shear strength on the sign of the shear stress. Interactions amongst stress components are considered to be independent material properties, which is different from the earlier theories where interactions are either fixed or excluded.

The tensor polynomial failure criterion developed by Tsai and Wu accounts for the interaction effects among stress components and offers a significant improvement in operational simplicity over many other failure theories [46]. They postulate that the criterion in stress space consists of the sum of linear and quadratic invariant as follows :

$$F_{ij}\sigma_i\sigma_j + F_i\sigma_i = 1, \qquad i,j = 1,2,3,4,5,6 \tag{2.27.}$$

Where F_{ij} and F_i are strength parameters associated with the failure criterion and σ_{ij}, σ_i are the stress components in the material axes.

Certain stability conditions are incorporated in the strength tensors. The magnitude of interaction terms are constrained by the following inequality :

$$F_{ii}F_{jj} - F_{ij}^2 \geq 0 \qquad (2.28.)$$

If this condition is not respected, the failure envelope becomes hyperbolic.

For a thin orthotropic ply under plane stress relative to the symmetry axes x-y, equation (2.27.) assumes the following form :

$$F_{xx}\sigma_x^2 + F_{yy}\sigma_y^2 + 2F_{xy}\sigma_x\sigma_y + F_{ss}\sigma_s^2 + F_x\sigma_x + F_y\sigma_y + F_s\sigma_s = 1 \qquad (2.29.)$$

The stress terms which are linear represent various tensile and compressive strengths and the terms which are quadratic represent an ellipsoid in stress space. The strength parameters can be determined from the material strength and are given by :

$$\begin{aligned} &F_{xx} = 1/XX', \qquad F_{yy} = 1/YY', \qquad F_{ss} = 1/S^2 \\ &F_x = 1/X - 1/X', \qquad F_y = 1/Y - 1/Y', \qquad F_s = 0 \end{aligned} \qquad (2.30.)$$

The term that involves F_{xy} represents an interaction between normal stresses in a fashion which is different from the ordinary shear stress. F_{xy} is a constant, similar to K_2 in the modified Marin equation (Eq. 2.26) whose magnitude is determined from complex stress data, that attempts to provide better correlation between experimental and theoretical results. Only one F_{xy} value is necessary to define the failure surface, but since its magnitude determines the inclination and semi-axis of the ellipse, then care is required in its determination.

The magnitude of F_{xy} can be determined from any test that produces a complex stress state in the principal material directions such as off-axis uniaxial stress tests and biaxial stress tests. Since the influence of F_{xy} on the failure envelope is large, then the most accurate method

of evaluating F_{xy} must be selected. F_{xy} should be unique for a particular material, but due to material property scatter and testing methods, and since the theories are phenomenological, then, in practice, this is not necessarily true. Numerous F_{xy} values can be obtained for the same material from different tests and hence, a technique is required to discriminate between determination methods.

Wu [54] concluded that uniaxial off-axis tests yield poor F_{xy} sensitivity. He attempted to optimize F_{xy} by accounting for experimental scatter and concluded that it is best determined from biaxial stress tests.

It has generally been found that the value of F_{xy} is very sensitive and dependent on the nature of the type of test employed. Some authors [44] have suggested it be set equal to zero which is physically unjustified. Wu and Stachurski [55] proposed yet another way of defining F_{xy} which is the following :

$$F_{12} = \frac{-1}{F_{11} + F_{22}} \tag{2.31.}$$

The absolute interaction term, or its normalized term F^{*}_{xy}, can be determined only by biaxial test

$$F_{xy} = F^{*}_{xy} [F_{xx} F_{yy}]^{1/2} \tag{2.32.}$$

The numerical value of the normalized term can be -1/2 for the generalized Von-Mises criterion, and zero for approximately the Hill/Hoffman criterion. In this project, $F^{*}_{xy} = -1/2$ had been used.

Since each combination of stress components in equation (2.27.) reaches its maximum when the left-hand side reaches unity. We can write equation (2.27.) under following form :

$$[F_{ij}\sigma_i\sigma_j]R^2 + [F_i\sigma_i]R = 1, \qquad i,j = 1,2,3,4,5,6 \tag{2.33.}$$

The value of the stress components in equation (2.33.) are that of the applied stress. We can substitute equation (2.33.) in to (2.27.) and achieve :

$$AR^2 + BR - 1 = 0 \tag{2.34.}$$

with $A = F_{ij}\sigma_i\sigma_j$ and $B = F_i\sigma_i$

We only need to solve the quadratic equation in the stress/strength ratio R. The correct answer is the positive square root in the quadratic formula :

$$R = -(B/2A) + [(B/2A)^2 + 1/A]^{1/2} \tag{2.35.}$$

When the applied stress is unity, the resulting strength ratio R is the strength.

2.1.6. Criteria considering different modes of failure

Puck and Schneider [42] put forward a failure criterion for a unidirectional fiber reinforced laminate which also compares three possible modes of failure : fiber fracture, matrix failure and failure of the fiber/matrix interface. A micro-scale analysis of the stresses acting on fiber, matrix and interface is propounded with the following bases and failure criterion :

(i) Fiber failure – maximum longitudinal stress :

$$\frac{\sigma_1}{X_f} = 1 \tag{2.36.}$$

where X_f is ultimate strength of fiber.

(ii) Matrix failure – distortion energy :

$$\left(\frac{\sigma_1}{X_m}\right)^2 - \frac{1}{3}\frac{\sigma_1\sigma_2}{X_m Y_m} + \left(\frac{\sigma_2}{Y_m}\right)^2 + \left(\frac{\sigma_{12}}{S_m}\right)^2 = 1 \qquad (2.37.)$$

where X_m, Y_m and S_m are ultimate strengths of matrix.

(iii) Fiber/matrix interface failure – assumed combination of maximum transverse stress and maximum shear stress of parabolic form :

$$\frac{\sigma_2}{Y_i} + \left(\frac{\sigma_{12}}{S_i}\right)^2 = 1 \qquad (2.38.)$$

where subscript i refers to interface failure. The strengths of fiber and matrix have used in this criterion. Hütter has proved that this criterion will be not efficient when using the laminated composites [38].

It is considered unidirectional composite isotropic in (y,z) plane. Hashin and Rotem [16] have stipulated that criterion of failure has to be a invariant function of stresses in this plane. They have distinguished four possible modes of failure, such as fiber fracture in tension or compression as well as matrix fracture in tension or compression. Their criterion is a combination of four corresponding sub-criteria and four modes of failure were also enumerated as following :

$$\left(\frac{\sigma_1}{X}\right)^2 + \left(\frac{\sigma_{12}}{S}\right)^2 = 1$$

$$\frac{\sigma_1}{X'} = 1 \qquad (2.39.)$$

$$\left(\frac{\sigma_2}{Y}\right)^2+\left(\frac{\sigma_{12}}{S}\right)^2=1$$

$$\left(\frac{\sigma_2}{2S}\right)^2+\left[\left(\frac{Y'}{2S}\right)^2-1\right]\frac{\sigma_2}{Y'}+\left(\frac{\sigma_{12}}{S}\right)^2=1$$

Fourth sub-criterion is rarely implicated since matrix attains rarely failure in compression. In the case of loading in (x, y) plane, Hashin-Rotem's criterion is equivalent to maximum stress criterion with identical transverse strength in tension and compression.

2.1.7. Conclusion

Some of the best known failure theories for anisotropic materials were reviewed in this chapter. Failure criteria are empirical and phenomenological. They can not be readily related to failure modes. The physical phenomena of the failure of composites are much too complicated to be described by any of the simple criteria mentioned in this chapter. Attention was focused on the fact that the quadratic formulations of the tensor polynomial criteria are very sensitive to the value of the interaction term F_{xy}. Figure 2.3 shows the effect of F_{xy} on the Tsai-Wu failure envelopes for $\sigma_6 = 0$ and $X = Y = X' = Y'$. This criterion was used the most because of its easy application, continuous extension to a last ply failure prediction [47], mathematical simplicity, invariance and internal consistency.

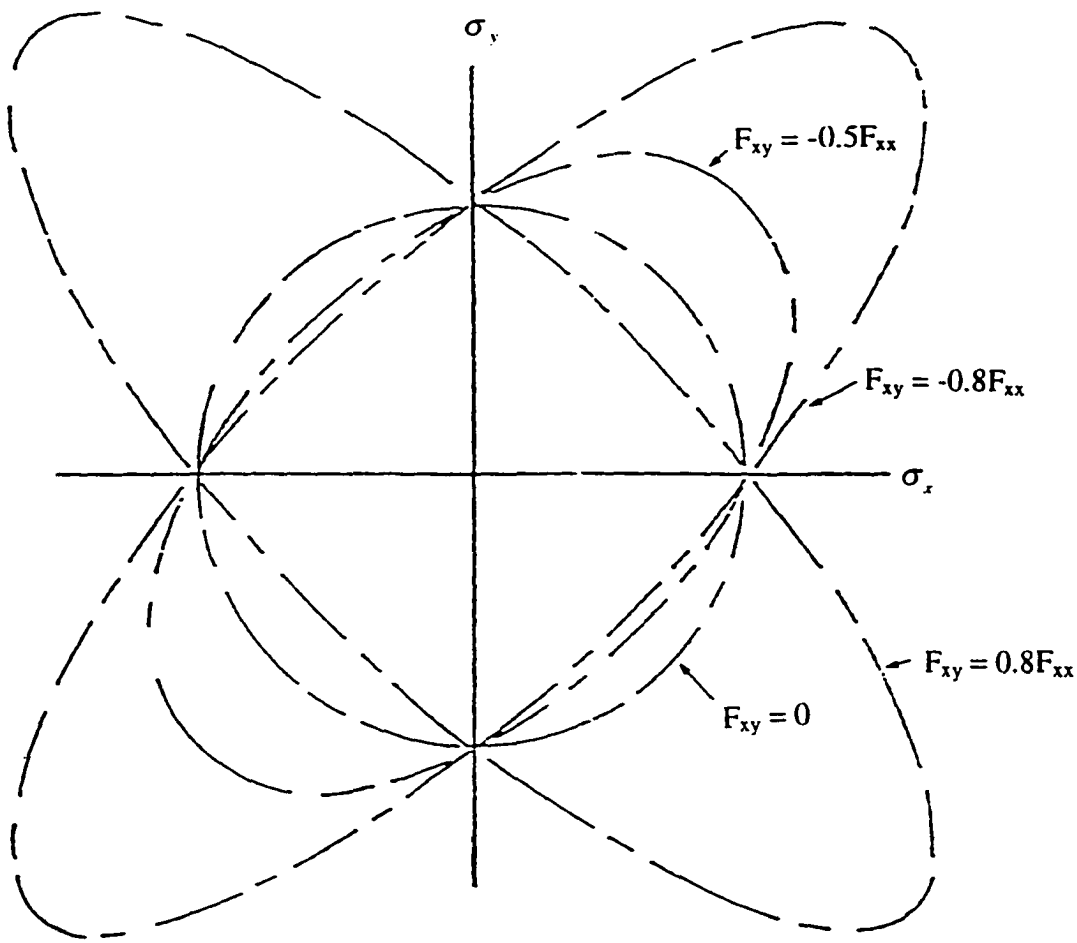

Figure 2.3 : Effect of the interaction parameter F_{xy} on the Tsai-Wu failure envelope

for $X = Y = X' = Y'$ and $\sigma_s = 0$ (reproduced from Ref. [11])

2.2. FABRIC STRUCTURE AND MODELS

2.2.1. Introduction

The various types of fabric structures can be identified by the pattern of their repeating regions. They are characterized by a geometrical parameter, n_g, that denotes that a warp thread is interlaced with every n_g-*th* fill thread. Figure 1.1 has presented an example of various types of woven fabric.

Recently, there are normally five different models which are then employed to approximate the elastic and strength behavior of composites: one model for laminated composite and four models for woven fabric composites.

In the case of laminated composites, the model is called laminated mechanical model is applied and mechanical behavior of laminated composites is based on the mechanical properties of each constituent unidirectional ply.

In the first model for woven fabrics, known as the mosaic model, a fabric composite is idealized as an assemblage of asymmetrical cross-ply laminates [19, 21]. Based upon the assumptions of the iso-stress and iso-strain, bounds of elastic moduli are derived and they provide an approximate method for predicting the elastic moduli.

In the second model for woven fabrics, the mosaic model is modified to take into consideration the effect of fiber undulation and continuity on composite stiffness. A one-dimensional strip of the fabric composite forms the basis of the analysis and the classical laminated plate theory is applied to each infinitesimal piece of the composite plate. This model has been extended to investigate the bi-linear or knee behavior of the stress-strain relations of plain weave composites.

The concept of the third model for woven fabrics is developed based on the findings of load transfer in satin weave composites [22]. The region with straight threads surrounding an undulated interlaced region has higher local in-plane stiffness than the latter and acts as a load-transferring bridge. This model has also been extended to the analysis of the knee behavior in satin weave composites where the same assumptions about internal failure are employed. This model has been also modified for treating hybrid woven composites and is called the "modified bridging model". The basic idea of the bridging action of the third model is preserved, although the geometry of this fourth model is much involved due to the complexity in the hybrid fabric structure. This model provides a significant improvement of the predictions of the simple bound results [21].

And last model for woven fabrics is called the sub-plies model which has been proposed for the characterization of the thermo-elastic properties for any deformed woven fabric composite [28-29, 50-52]. This work aims at applying the sub-plies model in the prediction of tensile and compressive strengths of orthogonal and non-orthogonal (deformed) woven fabric laminates. The effect of fiber undulation and yarns' interlacing on failure behavior are analyzed.

2.2.2. Laminated mechanical model

In the case of laminated composites, stiffness components are calculated by laminated mechanical model.

The generalized Hooke' s law relating stresses to strains can be written in contracted notation as :

$$\sigma_i = C_{ij}\varepsilon_j \tag{2.40.}$$

where σ_i are the stress components, C_{ij} is the stiffness matrix and ε_j are the strain components. The stiffness matrix C_{ij} has 36 constants, however due to symmetry ($C_{ij} = C_{ji}$), only 21 of the constants are independent.

A lamina is under a plane stress state when $\sigma_3 = \sigma_4 = \sigma_5 = 0$, and therefore only σ_1, σ_2 and σ_6 are presented, on axis stress-strain relation can be expressed by following [46]:

$$\begin{Bmatrix} \sigma_x \\ \sigma_y \\ \sigma_s \end{Bmatrix} = \begin{bmatrix} Q_{xx} & Q_{xy} & 0 \\ Q_{yx} & Q_{yy} & 0 \\ 0 & 0 & Q_{ss} \end{bmatrix} \cdot \begin{Bmatrix} \varepsilon_x \\ \varepsilon_y \\ \varepsilon_s \end{Bmatrix} \tag{2.41.}$$

The principal directions of orthotropy in an orthotropic material do not always coincide with the directions of the applied load. In fact, this would be the exception rather than the rule and quite often we need to use some transformation relations in order to express the stresses in the required directions, i.e., the directions of orthotropy. This can be done using the following relations :

$$\begin{Bmatrix} \sigma_x \\ \sigma_y \\ \sigma_s \end{Bmatrix} = \begin{bmatrix} \cos^2\theta & \sin^2\theta & 2\sin\theta\cos\theta \\ \sin^2\theta & \cos^2\theta & -2\sin\theta\cos\theta \\ -\sin\theta\cos\theta & \sin\theta\cos\theta & \cos^2\theta - \sin^2\theta \end{bmatrix} \cdot \begin{Bmatrix} \sigma_1 \\ \sigma_2 \\ \sigma_6 \end{Bmatrix} \tag{2.42.}$$

where θ is the angle between the fibers and the loading direction. An example of lamina orientation is given in Figure 2.1 or we can write off-axis stress-strain relation for unidirectional composite in terms of stiffness as following way:

$$\begin{Bmatrix}\sigma_1\\ \sigma_2\\ \sigma_6\end{Bmatrix}=\begin{bmatrix}Q_{11} & Q_{12} & Q_{16}\\ Q_{21} & Q_{22} & Q_{26}\\ Q_{61} & Q_{62} & Q_{66}\end{bmatrix}\cdot\begin{Bmatrix}\varepsilon_1\\ \varepsilon_2\\ \varepsilon_6\end{Bmatrix} \tag{2.43.}$$

where :

$$Q_{11} = Q_{xx}\cos^4\theta + 2(Q_{xy} + 2Q_{ss})\sin^2\theta\cos^2\theta + Q_{yy}\sin^4\theta$$

$$Q_{12} = (Q_{xx} + Q_{yy} - 4Q_{ss})\sin^2\theta\cos^2\theta + Q_{xy}(\sin^4\theta + \cos^4\theta) = Q_{21}$$

$$Q_{22} = Q_{xx}\sin^4\theta + 2(Q_{xy} + 2Q_{ss})\sin^2\theta\cos^2\theta + Q_{yy}\cos^4\theta$$

$$Q_{16} = (Q_{xx} - Q_{xy} - 2Q_{ss})\sin\theta\cos^3\theta + (Q_{xy} - Q_{yy} + 2Q_{ss})\sin^3\theta\cos\theta = Q_{61}$$

$$Q_{26} = (Q_{xx} - Q_{xy} - 2Q_{ss})\sin^3\theta\cos\theta + (Q_{xy} - Q_{yy} + 2Q_{ss})\sin\theta\cos^3\theta = Q_{62}$$

$$Q_{66} = (Q_{xx} + Q_{yy} - 2Q_{xy} - 2Q_{ss})\sin^2\theta\cos^2\theta + Q_{ss}(\sin^4\theta + \cos^4\theta)$$

Applying the classical lamination theory, coefficients A_{ij}, B_{ij}, D_{ij} can be determined from the coefficients Q_{ij} [46] :

$$\begin{aligned} A_{ij} &= \sum_{k=1}^{N}(Q_{ij})_k(z_{k+1} - z_k)\\ B_{ij} &= \sum_{k=1}^{N}(Q_{ij})_k\left(z^2{}_{k+1} - z_k{}^2\right)\\ D_{ij} &= \frac{1}{3}\sum_{k=1}^{N}(Q_{ij})_k\left(z^3{}_{k+1} - z_k{}^3\right)\end{aligned} \tag{2.44.}$$

where :

N : total numbers of ply (or layer)

k : the k-th layer.

z : position of ply in z-direction.

The A_{ij} are called extensional stiffness, the B_{ij} are called coupling stiffness and the D_{ij} are the bending stiffness. If the coupling stiffness are non-zero, then we should expect an in-

plane loading to produce a coupled effect of bending as well as extension. This coupled effect can be prevented by constructing laminates which are symmetrical with respect to the middle surface (plane), in which case B_{ij} reach zero values.

And the equation (2.43.) can also be written by the following :

$$\begin{bmatrix} \varepsilon_j^0 \\ k_j \end{bmatrix} = \begin{bmatrix} a_{ij} & b_{ij} \\ b_{ij} & d_{ij} \end{bmatrix} \begin{bmatrix} N_i \\ M_i \end{bmatrix} + \Delta T \begin{bmatrix} a_i^{th} \\ b_i^{th} \end{bmatrix} \tag{2.45.}$$

Classical laminate theory is based on the assumption that inter-laminar stresses are negligible and, therefore, lamina stresses do not change if the stacking sequence is changed as long as the entire laminate remains symmetrical. However, it was observed experimentally that different stacking sequences produce different lamina stresses in symmetrical laminates which may indicate that interlaminar stresses have a rather measurable effect on the behavior of laminates.

2.2.3. Mosaic model

This model has been proposed by Chou [19]. It can only use in the case of woven fabrics consisting of two sets of yarns interlaced at a 90° angle : orthogonal woven fabrics (or non-deformed woven fabrics). Woven fabric is simplified as the Figure 2.4 by repetitive order of cross-ply laminates[0/90] and [90/0]. According to each pattern of cross-ply laminate that is defined by geometrical parameter n_g. Otherwise, the effect of fiber undulation and continuity on composite stiffness in this model were neglected.

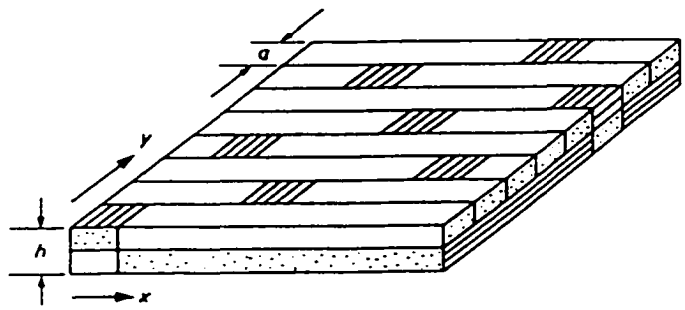

Figure 2.4 : Idealization for the mosaic model.

Furthermore, the state of strain ε_j^0 et k_j are considered uniform on all points of woven fabric structure. Average stresses $\overline{N_i}$ and moments $\overline{M_i}$ are defined by :

$$(\overline{N}_i, \overline{M}_i) = \frac{1}{n_g a}\left[\int_0^a (N_i, M_i)dx + \int_a^{n_g a} (N_i, M_i)dx\right] \qquad (2.46.)$$

where $n_g a$ is a unit of length and h is a thickness of fabric.

Substituting $\overline{N_i}$ and $\overline{M_i}$, into equation (2.43.), it is obtained the rigid coefficients $\overline{A_{ij}}$, $\overline{B_{ij}}$ and $\overline{D_{ij}}$ that can be expressed by :

$$\begin{aligned} \overline{A_{ij}} &= A_{ij} \\ \overline{B_{ij}} &= \left(1 - \frac{2}{n_g}\right) B_{ij} \\ \overline{D_{ij}} &= D_{ij} \end{aligned} \qquad (2.47.)$$

We can see that $\overline{A_{ij}}$, $\overline{B_{ij}}$ and $\overline{D_{ij}}$ can be calculated from the A_{ij}, B_{ij} and D_{ij} of laminates (Eq. 2.44).

$\overline{B_{ij}}$ represent the coupling stiffness between bending and extension, when $n_g = 2$ $\overline{B_{ij}}$ is equal to zero. Chou [7] has shown that with the mosaic model, the results were only correct for $n_g > 4$.

2.2.4. Fiber undulation model

Because the mosaic model can only apply for woven fabrics with $n_g > 4$, in order to use in the case of plain weave fabrics $n_g = 2$, Chou [22] has proposed a second model which is called the fiber undulation model. In this model, the effect of fiber undulation and continuity on composite stiffness have been considered.

This model based on the micro-mechanical behavior of woven fabrics, permits to integrate undulation form of structure. This undulation form is defined by three geometrical parameters $h_1(x)$, $h_2(x)$ and a_u as shown in Figure 2.5.

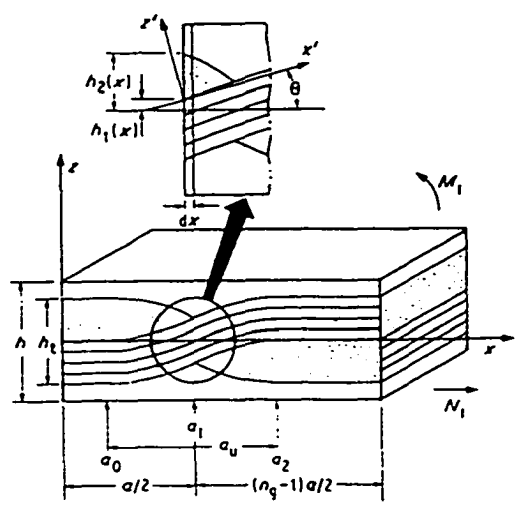

Figure 2.5 : Fiber undulation model (reproduced from Ref. [22])

where $h_1(x)$ and $h_2(x)$ vary between $-h_f/2$ and $h_f/2$, and in the undulation region ($a_2 \geq x \geq a_0$), they vary according to sinusoidal equation.

The fundamental assumption is that the classical laminate theory is applicable to each infinitesimal piece of the strip along the undulation direction. The average coefficients of compliance are calculated by :

$$\overline{a_{ij}} = \left(1 - \frac{2a_u}{n_g a}\right) a_{ij} + \frac{2}{n_g a} \int_{a0}^{a2} a_{ij}(x)dx$$

$$\overline{b_{ij}} = \left(1 - \frac{2}{n_g a}\right) b_{ij} + \frac{2}{n_g a} \int_{a0}^{a2} b_{ij}(x)dx \qquad (2.48.)$$

$$\overline{d_{ij}} = \left(1 - \frac{2a_u}{n_g a}\right) d_{ij} + \frac{2}{n_g a} \int_{a0}^{a2} d_{ij}(x)dx$$

where $a_{ij}(x)$, $b_{ij}(x)$ and $d_{ij}(x)$ are calculated from the a_{ij}, b_{ij} and d_{ij} of laminates which is modified the position x and volume ratio between the fibers and the resin.

This model can use for woven fabrics with $n_g < 4$ and gave the good results [22]. Obviously, using this model is more difficulty than using the mosaic model, but it is efficient specially for plain weave and it is also only used for orthogonal woven fabric composites.

2.2.5. Bridging model

This model [22] is desirable in view of the fact that the interlaced regions in a satin are separated from each other. The geometry of the model is shown in Figure 2.6.

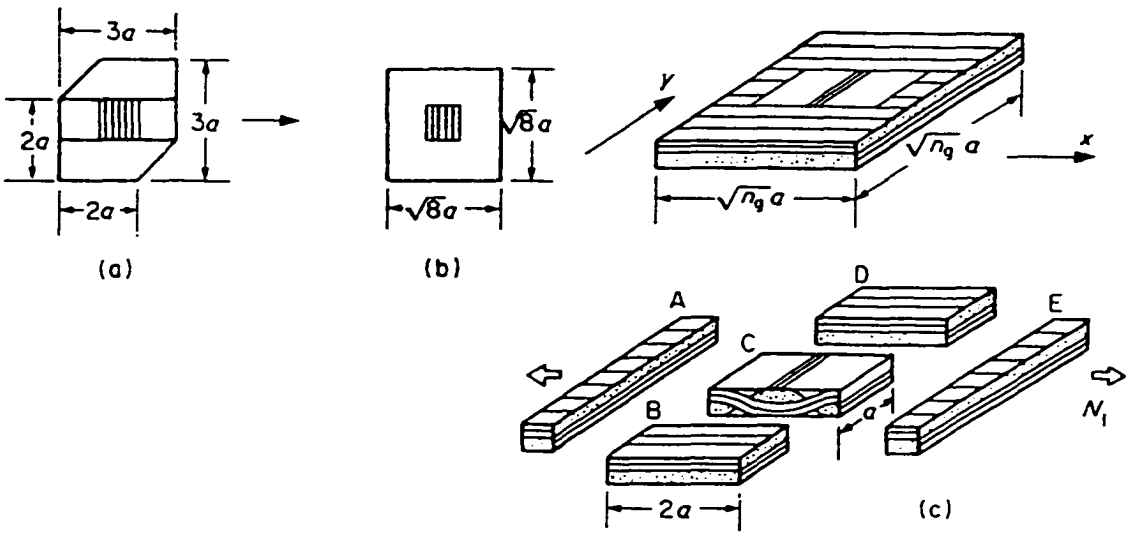

Figure 2.6 : Bridging model (a) shape of a repeating unit of 8-harness satin;

(b) modified square shape and (c) basic idealization (reproduced from Ref. [22])

where the shapes of the repeating regions are modified. This model is valid for only satin weave where $n_g > 4$. The four regions labeled by A, B, D, E consist of straight fill thread, and hence, can be regarded as pieces of cross-ply laminates of thickness h. Region C has an undulated fill and the continuity and undulation in the warp are ignored. The latter effect is expected to be small because an applied load is in the fill direction. The in-plane stiffness in region C where $n_g = 2$ is found to be much lower than that of a cross-ply laminate where $n_g \rightarrow \infty$. Therefore, regions B and D carry higher loads than region C, if we assume that those three regions have the same averaged strain and curvature.

The reason why the fiber undulation model is effective for plain weave composites whereas the bridging model is valid for satin weave composites can be explained as following : there are no straight thread regions surrounding an interlaced region and the one-dimensional

distribution of in-plane stiffness is identical in each thread in a plain weave composite. It can be expected, therefore, that no bridging effect occurs in the plain weave composite and that each thread carries the same in-plane force. Hence, the one-dimensional and bridging approaches are suitable for the plain and satin weave composites, respectively.

2.2.6. The sub-plies model

Figure 2.7 shows the sub-plies model. In this model the fabric, consisting of a warp and a weft, is replaced by four fictional unidirectional laminae with orthotropic properties [28-29, 50-52] that are laid up in an antisymmetric configuration $[0_{h1}/90_{h2}/0_{h2}/90_{h1}]$. By choosing adequate thickness for the sub-plies, the stiffness coefficients, $\overline{A_{ij}^S}$, $\overline{B_{ij}^S}$ and $\overline{D_{ij}^S}$, of the fabric composite can be obtained. Since the configuration of the sub-plies model is anti-symmetric, the thickness of the plies can be defined by a fictive thickness, e, which is a function of the fabric thickness t and the geometrical parameter n_g of the fabric [28-29, 50-52].

$$e = t_o \sqrt{\frac{1}{n_g}} \tag{2.49.}$$

The stiffness coefficients of the sub-plies laminate, $\overline{A_{ij}^S}$, $\overline{B_{ij}^S}$ and $\overline{D_{ij}^S}$, can then be obtained from the classical laminated plates theory.

To predict the failure envelope of the composites made, the strength coefficients of the constituent ply such as: longitudinal tensile and compressive strengths (X, X'), transverse tensile and compressive strengths (Y, Y') and shear strength (S) are needed. In previous works [28-29, 50-52], a special procedure has been proposed to determine the thermo-elastic coefficients of the fictional constituent plies. In this work, the same approach was used to

determine the strength coefficients and the results are compared with that measured from unidirectional composites and on cross-ply $[0/90]_s$ laminates.

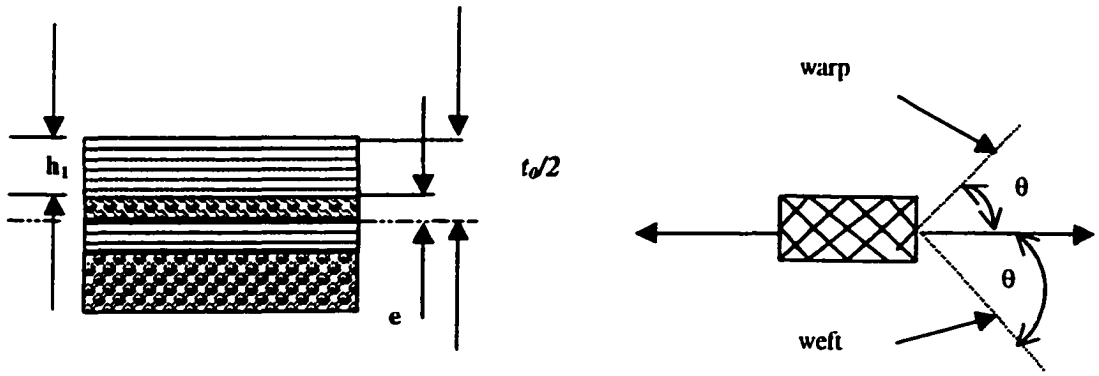

Figure 2.7 : Sub-plies model

Chapter 3

EXPERIMENTAL

3.1. MATERIALS

There are two types of woven fabric that were used in this study, plain weave and 8-harness satin fabrics. The samples were made with a glass-fiber woven fabric (WR180Z) and an unsaturated polyester resin (AK2100) supplied by Armkem Canada. All the specimens were fabricated by using fiber and resin via the wet lay-up process with a fiber volume content of about 48-52 %. The fiber volume fraction of the molded samples was always verified after molding by burning off the resin and measuring its percentage in the specimen.

Three types of plaque with the same thickness of 2 mm were prepared: a) unidirectional plaques; b) cross-ply $[(0/90)_n]_s$ plaques; c) plain weave fabric composite and the other type of plaque was fabricated by 8 harness satin with the thickness 1.2mm was also used. In this work, unidirectional plies were made by the same E-glass fiber with the same properties, such as the thickness and width of bundle, tow size, density ... etc. In order to verify the predicted results, deformed samples were also fabricated with various angles such as $\theta = 28^0, 31^0, 36^0, 45^0, 51^0$ and 57^0. These non-orthogonal woven laminates were made by deforming the orthogonal interlaced yarns of the fabric by in-plane shearing to different angles before molding (Figure 3.1).

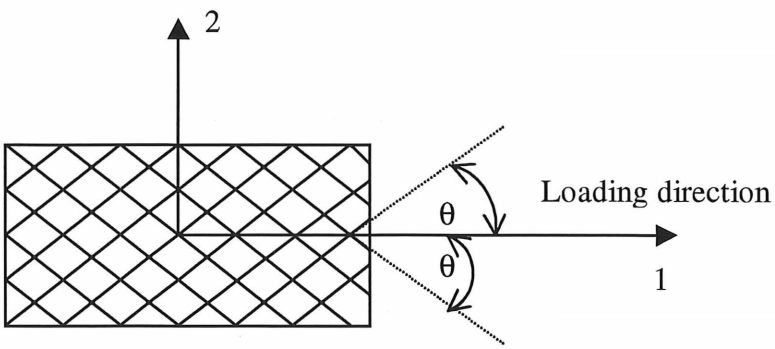

Figure 3.1: Deforming the orthogonal interlaced yarns of the fabric by in plane shearing to different angles.

3.2. SAMPLE PREPARATION AND TESTING

Tensile tests were carried out according to the ASTM D-3039 standard [1, 23]. The specimen dimensions were 203mm (8.0 in.) by 25.4mm (1.0 in.) with a test section length of 127mm (5.0 in.). End tabs were bonded to the specimen as recommended in [1, 23] (Figure 3.2).

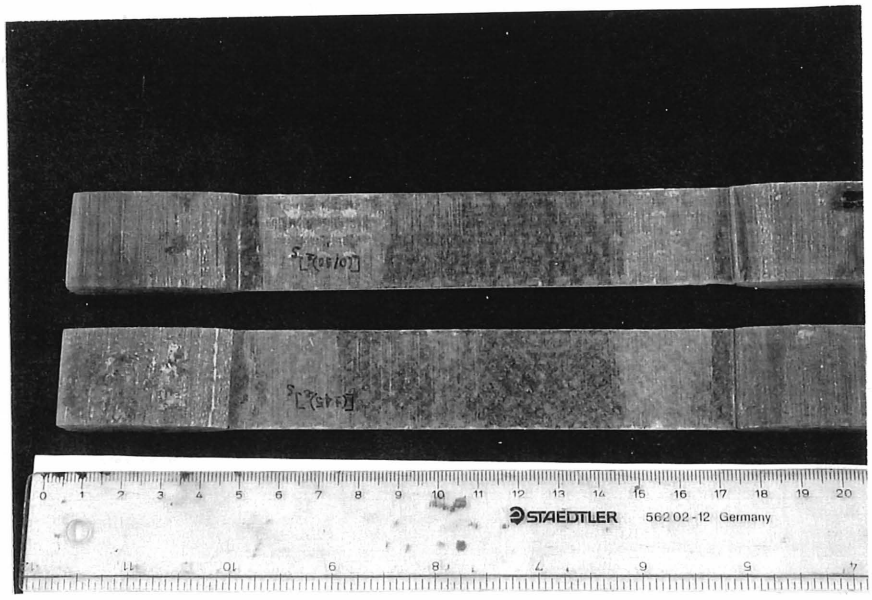

Figure 3.2: Tensile specimen

The specimen edges were carefully polished to eliminate any possible damage and to insure the required dimensions of the samples. The tensile tests were performed using wedge-section grips. The specimens were loaded monotonically to failure at a recommended rate of 1.27mm/min (0.05 inches per minute). Strain gages (one in the longitudinal and one in the transverse direction) were bonded to the specimen at the center of the test section and monitored during the test. The elastic properties were determined by at least 25 data, measured in the linear response region as recommended in [30].

The compressive tests were carried out according to the ASTM D-3410-87 standard (Celanese compression test fixture) [1]. The Celanese test fixture employs truncated conical friction grips contained in matching cylindrical end fittings. Colinearity of the cylindrical end fittings was insured by a hollow cylinder, which contains the fittings. The gripping devices of the Celanese allow the ratio of the normal and the shear loading to remain approximately the same for the entire loading process.

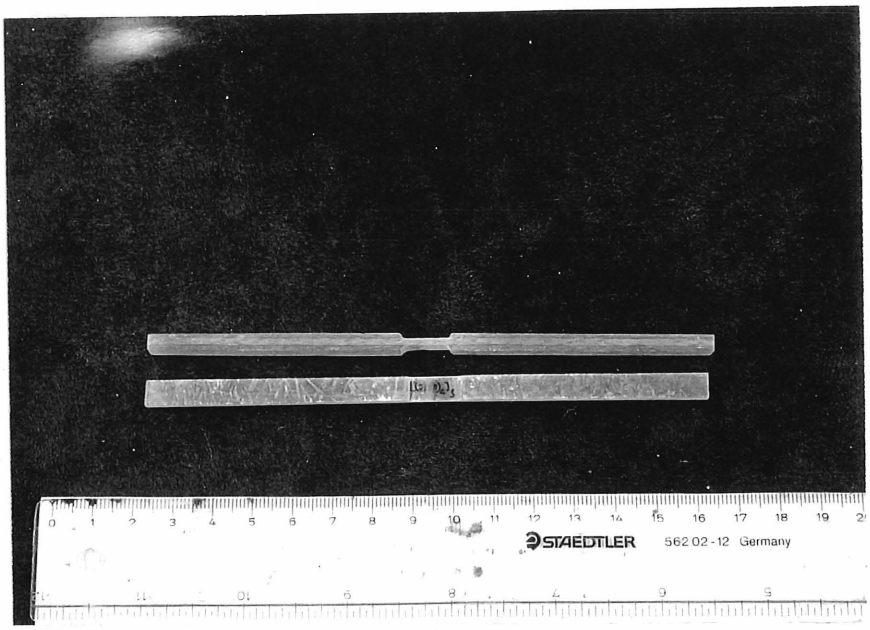

Figure 3.3: Compressive specimen

The specimens were cut from the molded plaques to the dimensions of 141mm (5.5 in.) by 6.4mm (0.25 in.) with a test section length of 12.7mm (0.5 in.). End tabs were also used in these specimens (Figure 3.3). The specimens were loaded at a cross-head speed of 0.5 mm/min (0.02 inches per minute).

We know that the lamina properties in the plane of lamination (1-2) are known as the in-plane shear properties, while the properties in the (1-3) and (2-3) planes are known as interlaminar shear properties. Shear tests for the laminate composite have generally been restricted to the evaluation of properties in the plane of the laminate. There are four generally accepted test methods for the evaluation of lamina in-plane shear properties. They are the $[(45/-45)]_s$ coupon test, the off axis coupon, the rail shear test method and the torsion test [23]. The 10-degree angle was chosen to minimize the effects of longitudinal and transverse tension components on the shear response. In the case of graphite-epoxy composite the 10-degree off-axis test yields a higher initial modulus, while the $[(45/-45)]_s$ laminate yields a higher strength. The $[(45/-45)]_s$ laminate test yields considerably more of the shear stress-strain curve than the 10-degree off-axis test [23]. The most simple tests to perform are the tensile test using the off-axis and the $[(45/-45)]_s$ coupons. Although Chamis and Sinclaire have recommended the 10-degree off-axis test for determining lamina shear properties [6] but the results for the 15-degree off-axis test indicated that the ultimate shear strength determined by the 15-degree test and the $[(45/-45)]_s$ tensile test compare quite favorably [41]. The $[(45/-45)]_s$ tensile test was also used popularly to determine the shear strength [9, 27] because it is simple and easy to use. Specially, when the difference of the shear strength between using $[(45/-45)]_s$ tensile test and $[(45/-45)]_s$ compressive test is not important, the shear strength that is determined from the $[(45/-45)]_s$ tensile test is acceptable. The $[(45/-45)]_s$ laminate tensile test has been suggested

to be a promising test method for the complete shear characterization of woven fabric composite [14]. The shear strength in this study is therefore determined from the $[(45/-45)]_s$ tensile test as proposing in [9, 27] and [14].

All the tests were carried out on Instron 4206 and Instron TTD-3025 machines. All the results were obtained from the average measurements of 5-8 samples. The scatters of specimens have been presented in the next chapter.

Chapter 4

DETERMINATION OF STRENGTH COEFFICIENTS

4.1. MODELING OF DEGRADED PLIES

In a laminated composite subjected to loading, the ply with the lowest strength will fail first. This initial failure defines the inner failure envelope of the composite. Once the applied stress exceeds the initial failure, a laminate may or may not be able to sustain additional load. Various approaches to rationalize the lower limit and the ultimate strengths for laminated composites have long been published. In these approaches, matrix degradation models have been proposed to distinguish the plies with cracks due to initial failure from the intact ones [39, 40, 47]. A ply or ply group with cracks will change the internal stress distribution of the laminate. A ply with transverse cracks will sustain lesser load. The effective stiffness of the laminate will therefore be reduced, but not as much as if the whole ply is removed from the laminate.

Because conventional stress analysis like laminated plate theory is limited to a continuum or plies without cracks, it has been proposed [47] to replace the cracked plies with a continuum of lower stiffness coefficients so that the conventional stress analysis can be applied. In fact, the observed stiffness of the laminate having partially and totally degraded plies is used to estimate the degree of the ply stiffness reduction. The replacement of cracked

plies by quasi-homogeneous plies has been done semi-empirically. A degradation factor *(DF)* has been proposed to apply directly to the stiffness and strength coefficients of the unidirectional plies [47]. Tsai has shown that this matrix degradation factor only effects on last ply failure in the principal strain plane (see page 12-7 in [47]). When the degradation factor *(DF)* is unity, there is no degradation and the first ply failure envelope is recovered. In the other case when the degradation factor *(DF)* approaches zeros, a maximum strain envelope is recovered. In order to avoid singularity, it has also been shown that the *(DF)* should be greater than 0.01. In this approach, the reduction of the matrix modulus is considered to affect the transverse modulus, E_y, the shear moduius, E_s, and the Poisson's ratio, ν_{xy}.

$$
\begin{aligned}
E_y &= (DF)E_Y^{\circ} \\
E_s &= (DF)E_s^{\circ} \\
\nu_{xy} &= (DF)\nu_{xy}^{\circ} \\
X' &= (DF)^{0.2}X'^{\circ} \\
F_{xy}^{*} &= (DF)\,F_{xy}^{*\circ}
\end{aligned}
\tag{4.1}
$$

where the superscript zero denotes the property of the intact plies, and F_{xy}^{*} is the coupling term in the quadratic criterion.

For glass/epoxy laminated composite the value of *(DF)* has been experimentally determined to be between 0.07 to 0.08. As a first approximation we selected a value of *(DF)* = 0.1 for this polyester/glass composite. In order to verify the effect of *(DF)* on the values of ultimate strengths of the composite a value of *(DF)* = 0.2 was also used and this effect will be discussed later.

In order to use this approach, the elastic and strength properties of the constituent fictional ply in Figure 2.7 must be known. Furthermore, it has been shown that in a laminated composite, the presence of adjacent plies alters the in-situ strength of the lamina [53]. Consequently, it is necessary to verify the stiffness and strength coefficients that should be used for the equivalent constituent plies in the sub-plies model. Measurements for such verification were thus carried out on unidirectional samples, cross-ply laminates samples, as well as samples made of the woven fabric composite (plain weave and 8-harness fabric composites).

4.2. MEASUREMENTS USING PLAIN WEAVE FABRIC COMPOSITE

It has been shown [28, 51-52] that, by measuring the properties of samples cut out in 0° and 45° directions, from the molded plaques of the plain weave fabric composite, the thermoelastic properties of the fictional constituent plies in Figure 2.7 can be determined. . Considering that the $[(0/90)_m]_s$ or $[(45/-45)_m]_s$ samples are replaced by the sub-plies model, $[(0_{h1}/90_{h2}/0_{h2}/90_{h1})_m]_s$ or $[(45_{h1}/-45_{h2}/45_{h2}/-45_{h1})_m]_s$, the laminate longitudinal Young's modulus, $E_{[0/90]}$, and the Poisson's ratio, $\nu_{[0/90]}$, can be calculated by using the classical laminate theory. The final equations are expressed as :

$$E_{[0/90]} = \frac{Q_{xx[eq]} + Q_{yy[eq]}}{2} - \frac{2Q^2_{xy[eq]}}{Q_{xx[eq]} + Q_{yy[eq]}} \qquad (4.2.)$$

$$\nu_{[0/90]} = \frac{2Q_{xy[eq]}}{Q_{xx[eq]} + Q_{yy[eq]}} \qquad (4.3.)$$

$$E_{[+45/-45]} = \frac{4\,Q_{ss[eq]}\,(Q_{xx[eq]}+Q_{yy[eq]}+2Q_{xy[eq]})}{Q_{xx[eq]}+Q_{yy[eq]}+2Q_{xy[eq]}+4Q_{ss[eq]}} \qquad (4.4.)$$

$$\nu_{[+45/-45]} = \frac{Q_{xx[eq]}+Q_{yy[eq]}+2Q_{xy[eq]}-4Q_{ss[eq]}}{Q_{xx[eq]}+Q_{yy[eq]}+2Q_{xy[eq]}+4Q_{ss[eq]}} \qquad (4.5.)$$

In the above equations, $Q_{xx[eq]}$, $Q_{yy[eq]}$, $Q_{xy[eq]}$ and $Q_{ss[eq]}$ are the equivalent on-axis stiffness coefficients of the constituent fictional plies shown in Figure 2.7. In fact, only three out of the above four equations are independent of each other because of the relation:

$$\frac{E_{[0/90]}}{1-\nu_{[0/90]}} = \frac{E_{[+45/-45]}}{1-\nu_{[+45/_{45}]}} \qquad (4.6.)$$

From the sub-plies model shown in Figure 2.7, *[0/90]* and *[45/-45]* in the above equations correspond to the warp and weft directions of the fabric. Where $E_{[0/90]}$ and $\nu_{[0/90]}$ are the Young ' s modulus and the Poisson ' s ratio that were determined from the tensile test on $[(0/90)]_s$ specimen; $E_{[45/-45]}$ and $\nu_{[45/-45]}$: the Young ' s modulus and the Poisson ' s ratio were determined from the tensile test on $[(45/-45)]_s$ specimen.

Therefore, another equation must be found to solve four unknown stiffness coefficients, $Q_{xx[eq]}$, $Q_{yy[eq]}$, $Q_{xy[eq]}$ and $Q_{ss[eq]}$. It is thus assumed that the effect of fibre undulation on the transverse Young's modulus of the constituent plies in the sub-plies model is negligible. This assumption leads to:

$$E_{y[eq]} = E_{y[unidir]} = Q_{yy[eq]} - \frac{Q^2_{xy[eq]}}{Q_{xx[eq]}} \qquad (4.7.)$$

The results of these measurements, determined by the least squares fit of the initial slopes of the stress-strain data, are given in Table 4.1.

Table 4.1 : Elastic properties of laminated and woven fabric composites

Specimens	PW fabric composite		8-HS fabric composite		Laminated composite	
	E (GPa)	ν	E (GPa)	ν	E (GPa)	ν
$[(0/90)_n]_s$	22.251	0.128	23.166	0.13	23.058	0.083
$[(45/-45)_n]_s$	14.937	0.463	15.858	0.437	14.083	0.489

With the assumption of $E_{y[eq]} = E_{y[unidir]}$ (Eq. 4.7.) the equivalent unidirectional properties of plain weave fabric composite derived from the measured data (Table 4.1) are presented in Table 4.2.

Table 4.2: Orthotropic mechanical properties of constituent ply in various structures.

Type of composite	E_x (MPa)	E_y (MPa)	E_s (MPa)	ν
Plain weave fabric composite	36.70	7.20	5.11	0.39
8-harness satin fabric composite	38.43	7.20	5.52	0.41
Unidirectional composite	39.06	7.20	4.73	0.25
Cross-ply laminates	38.64	7.20	4.73	0.26

To measure the strength coefficients of the constituent plies using these samples, it has been shown theoretically and experimentally [27, 39] that the stress-strain diagram of a cross-ply composite under tension is represented by a bilinear line. The intersection of the two straight segments was called the knee-point that indicates the failure of the 90° plies [39]. In the case of plain weave fabric composite, the tensile stress-strain curve for the sample in 0° direction is shown in Figure 4.1.

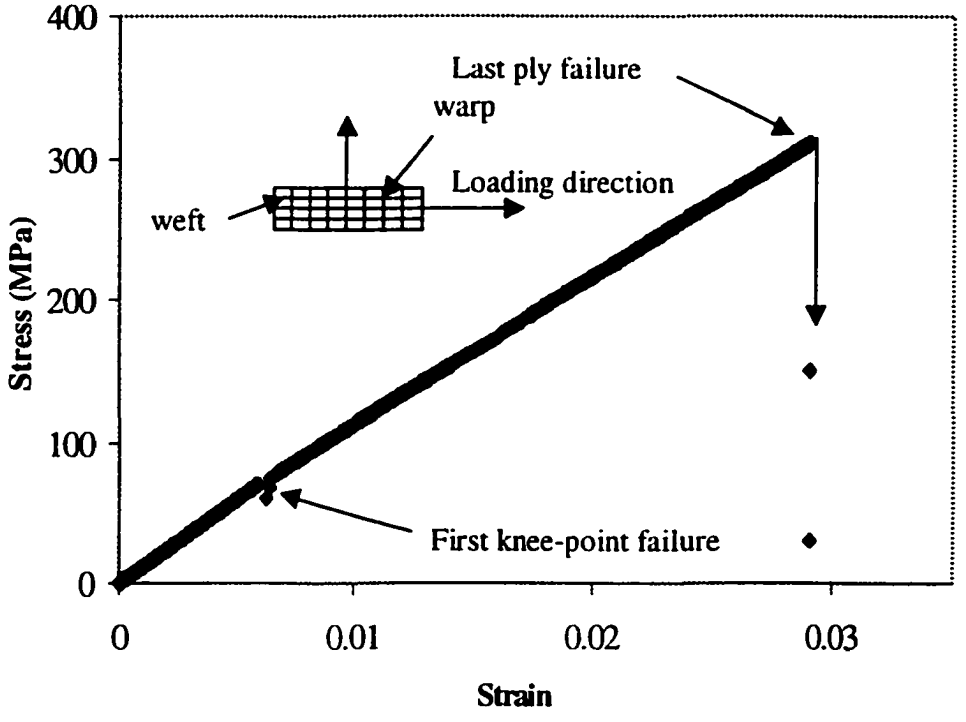

Figure 4.1 : Stress-strain curve of undeformed plain weave sample (orthogonal structure)

The result reveals that a bilinear behaviour is also observed, as in the case of cross-ply laminated. The intersection point of the two linear lines occurs at about 22-23% of the ultimate load. This value was used to determine the transverse strength coefficient (Y) of the fictional 90° ply in the sub-plies model. The ultimate load and deformation were used to calculate the longitudinal strength coefficient (X) of the 0° fictional ply, using a value of *(DF)* of 0.1.

In the compression tests the bilinear behaviour is not observed. The transverse compression strength coefficient of the fictional constituent ply cannot be directly determined from these samples. Thus, in order to predict envelopes of plain weave fabric composite the transverse compressive strength coefficient of the unidirectional ply was suggested using. The maximum load in the compression test was used to determine the longitudinal compression strength coefficient, by considering that the 90° plies had failed. Finally, the shear strength coefficient (S) was determined from the coupons cut out from the molded plaque at 45° as proposed in [14]. The strength coefficients of the constituent fictional ply in the sub-plies model, using these measured plain weave fabric composite results, are shown in Table 4.3.

Table 4.3: On-axis strength coefficients determined from measurements on laminated and woven fabric composites

Type of composite	X (MPa)	X' (MPa)	Y (MPa)	Y' (MPa)	S (MPa)
Plain weave fabric composite	548.70	306.44	23.74	115.35	40.49
8-harness satin fabric composite	669.26	380.02	24.74	115.35	38.35
Unidirectional composite	733.09	368.78	24.74	115.35	36.15
Cross-ply laminates	693.68	363.90	31.72	115.35	36.15

4.3. MEASUREMENTS USING 8-HARNESS SATIN FABRIC COMPOSITE

As in the case of plain weave fabric composite, measuring the properties of samples cut out in 0° and 45° directions from the molded plaques of the 8 harness satin fabric composite is necessary to determine the thermo-elastic properties of the fictional constituent plies in Figure 2.7. The results of these measurements, also determined by the least squares fit of the initial slopes of the stress-strain data, are also given in Table 4.1.

In the case of 8-harness satin fabric composite the tensile stress-strain curve for the sample in 0° direction is shown in Figure 4.2.

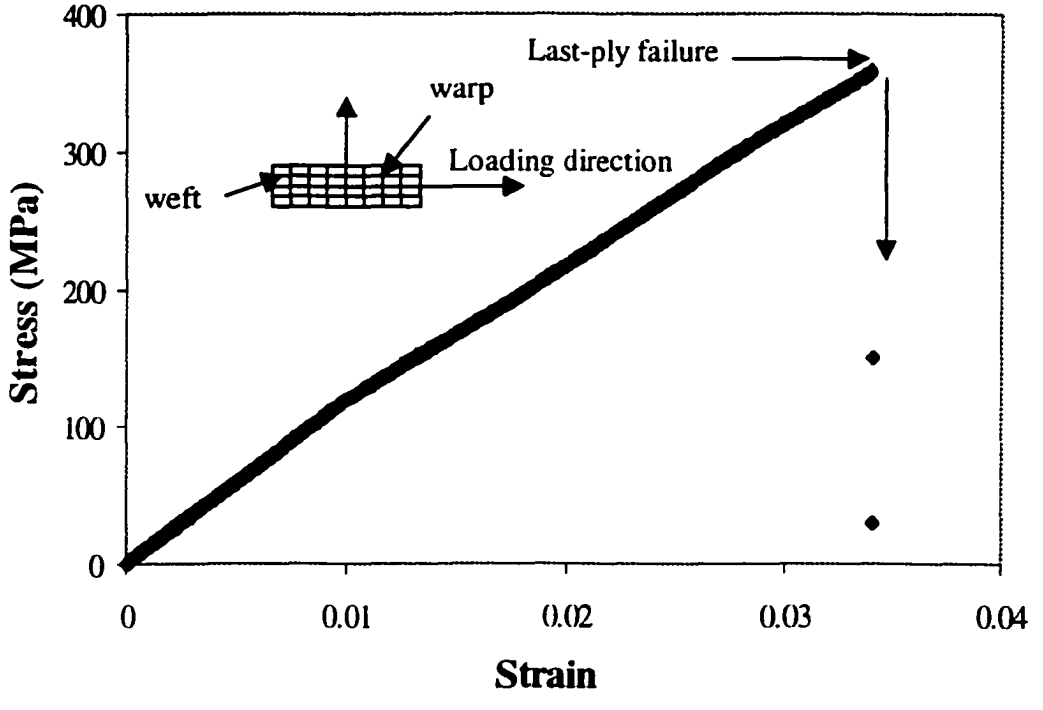

Figure 4.2 : Stress-strain curve of undeformed 8-harness satin sample (orthogonal structure)

The result reveals that a bilinear behaviour is not observed as in the case of cross-ply laminates and plain weave fabric composite. The difference of behaviours between these composites will be discussed later. Thus, the transverse tensile strength coefficient (Y) of unidirectional composite was used to calculate the envelopes of 8-harness satin composite. The ultimate load and deformation were used to calculate the longitudinal strength coefficient (X) of the 0° fictional ply, using a value of *(DF)* of 0.1 as in the case of plain weave fabric composite.

In the compression tests the bilinear behaviour is not also observed. As the case of plain weave fabric composite, the transverse compressive strength coefficient (Y') of unidirectional composite was also used to predict the envelopes of 8-harness satin fabric composite. The maximum load in the compression test was used to determine the longitudinal compression strength coefficient (X') and the shear strength coefficient (S) was also determined from the 45° coupons as plain weave fabric composite. The strength coefficients of the constituent fictional ply in the sub-plies model, using these measured 8-harness satin fabric composite results, are shown in Table 4.3.

4.4. MEASUREMENTS USING UNIDIRECTIONAL SAMPLES

The unidirectional samples were cut out from the unidirectional plaques, molded from the same composite. The elastic properties were also determined by the least squares fit of the initial slopes of the stress-strain data and are given in Table 4.2. The tensile, compressive and shear strength coefficients *X, Y, X', Y', S* of the unidirectional ply of the composite were also determined and are shown in Table 4.3. In this Table, the ultimate shear strength *S* was

obtained from the tensile test on $[(-45/45)]_s$ specimens, which are cut out in 45° from the $[0/90]_s$ plaques.

The results in Table 4.3 show that the longitudinal tensile strength coefficients X and X' of the fictional constituent ply of the plain weave fabric are much lower than that of the unidirectional composite. This could be explained by the undulation effect of fiber in the fabric system especially for plain weave fabric type. In the case of longitudinal tensile strength, since the degree of undulation of the fibers could not all be the same, fibers with less undulation would attain the ultimate strain first. Consequently, the volume fraction of fibers sustaining the load at ultimate fracture strain would be lower than that in a unidirectional composite. However, as it could be expected, the non-uniformity in fiber undulation has a lesser effect on the Young's modulus since in the elastic region, all the fibers contribute to the stiffness of the composite. It is also surprising to note that the transverse strength Y is equivalent to that measured by unidirectional samples. This result suggests that, unlike the constraint effect observed for the case of laminated laminae with different orientations, the presence of the warp fibers does not affect the transverse properties of the weft fibers and vice versa. Consequently, the transverse strength coefficient of the unidirectional composite can be used in the sub-plies model for woven fabric composites.

4.5. MEASUREMENTS USING SAMPLES CUT OUT FROM CROSS-PLY LAMINATES

Using the same approach proposed in [28, 51-52], as discussed above for the woven fabric laminates, the on-axis stiffness coefficients of the lamina can also be experimentally determined by measuring respectively the Young's modulus and Poisson's ratio of $[(0/90)_2]_s$ and $[(45/-45)_2]_s$ samples (Table 4.1). These samples were cut out in 0° and 45° from the

cross-ply plaques, molded from the same unidirectional composite. The stress-strain curve of the tensile test in 0° direction on cross-ply samples also showed the knee point due to matrix failure in the 90° layers. This point occurs at about 23-25% of the ultimate load, associated with fracture of the 0° plies. From these tests, the strength coefficients were determined in the same manner as it was done in the case of woven fabric composite. The compression test did not show a knee point and only the longitudinal compression strength coefficient (X') could be determined. These measured values are reported in Table 4.3. From these results, it can be seen, as expected, that the elastic properties of samples cut out from cross-ply laminates (Table 4.2) are nearly similar to that measured by the unidirectional samples and by the samples cut out from the woven fabric plaques. Comparing the woven laminated shear moduli with those of unidirectional composite, it is seen that woven laminate shear modulus values are appreciably higher. This could be because of the interlacing of strands in woven fabric composites as discussion in [35]. It is also observed that woven laminate Poisson' s ratio values are higher than those of the unidirectional composites. This is because of the undulation present in the case of woven fabric laminates. Specially, the transverse strength coefficient Y of cross-ply laminate is significantly higher. This result confirms the constraint effect of adjacent plies on the in-situ strength of the lamina. On the other hand, the values of X and X' are higher than that obtained from plain weave fabric samples, confirming the effect of fiber undulation on the strength performance of plain weave fabric composite. It is also observed that X and X' are slightly lower than that measured from unidirectional samples. This could be due to the fact that the fibers in the cross-ply plaques are less aligned than that in the unidirectional samples. This misalignment could be induced during the lay-up process.

Finally, the shear strength coefficient S is slightly lower than that measured on the woven fabric samples. This could be due to the interlacing effect of fibers in the fabric system.

4.6. CONCLUSION

From obtained results, the effect of the fiber undulation on the mechanical properties and on-axis strength coefficients can be clearly observed. The fiber waviness tends to reduce the longitudinal Young's modulus and the longitudinal tensile strength coefficient (X), and increase the Poisson's ratio value, the longitudinal shear modulus, and the shear strength coefficient.

Chapter 5

PREDICTION OF FRACTURE

5.1. TENSILE TEST

5.1.1. Stress-strain curves

5.1.1.1. Orthogonal woven composite

Several physical theories have been proposed to explain the non-linear stress-strain response of the laminated composites, the most widely accepted of there is the initial failure criterion [39, 45]. Discontinuous slopes in the stress-strain curve occur when one or more of the constituent layers have failed or there is phenomenon of breaking matrix. Tsai and Haln, in their works [5, 45], showed theoretically and experimentally that the stress-strain diagram of a cross-ply composite under tension is represented by a bilinear line. The intersection of the two straight segments implies the initial failure, and the intersection was called the knee-point [39].

In the case of plain weave fabric composite, the tensile stress-strain curve for laminate specimen tested at $\theta = 0^0$ is slightly non-linear, however, approximate bilinear segments as that in Fig.4.1 were considered. The point at which the two linear sections intersect is called the first knee-point and presents the fracturing of 90^0 plies. It is understood that the onset of the first knee is due to failure in the 90^0 layers and the ultimate failure of the laminate occurs

at the fracture strain of the 0^0 plies. Based on the experimental results, at the first linear end, the strain is about 0.25-0.27%, that is only about 22-23% of the ultimate. In the case of 8-harness satin fabric the first knee point is not observed as in the case of plain weave fabric composite and the stress-strain curve was shown in Figure 4.2.

5.1.1.2 Undeformed plain weave composite with $\theta = 45^\circ$

The stress-strain curve of undeformed plain weave specimen with $\theta = 45^\circ$ is shown in Figure 5.1.

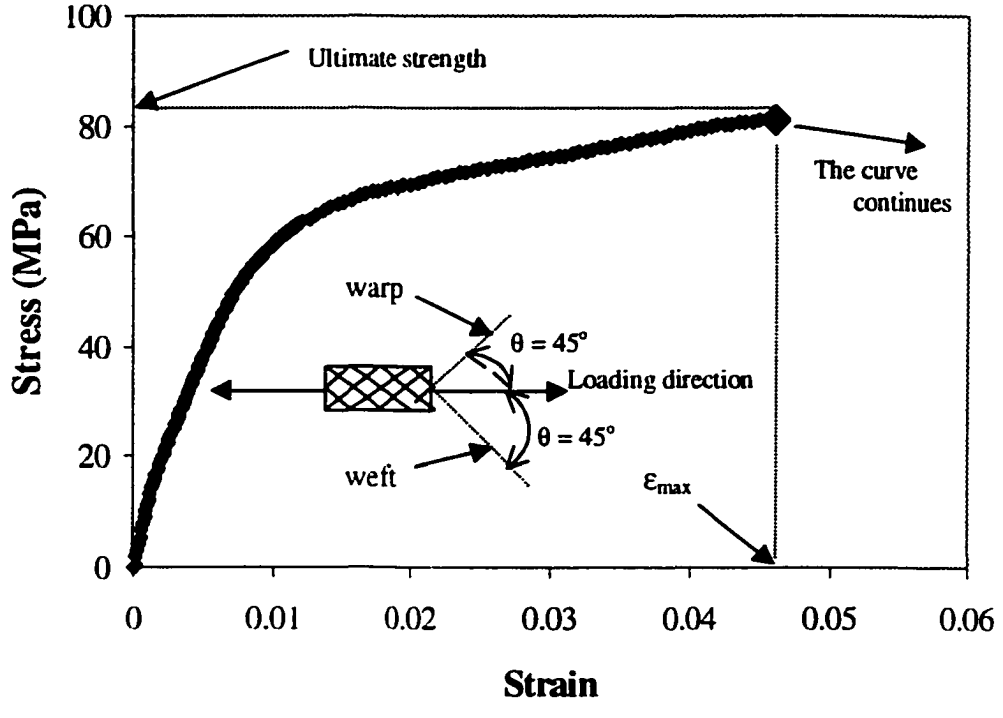

Figure 5.1: Tensile stress-strain curve of undeformed plain weave sample with $\theta = 45^\circ$

It can be seen that this graph has a non-linear behaviour and does not have any knee-point. In fact, it is possible that failure of the entire laminated composite occurs immediately after the initial failure of either layer and in this case the shear effect is dominant. Microscopic

observation at around of $0.5\varepsilon_{max}$ does not also show clear fracture in the warp or the weft direction but damage seems to occur in the form of matrix multi micro cracking.

Matrix multi micro cracking may lead to non-linear stress-strain behaviour of the laminates under off-axes loading conditions. In fact, under off-axis loading conditions interaction of several failure mechanisms results in a loss of stiffness before ultimate failure [25].

5.1.1.3 Deformed plain weave composites

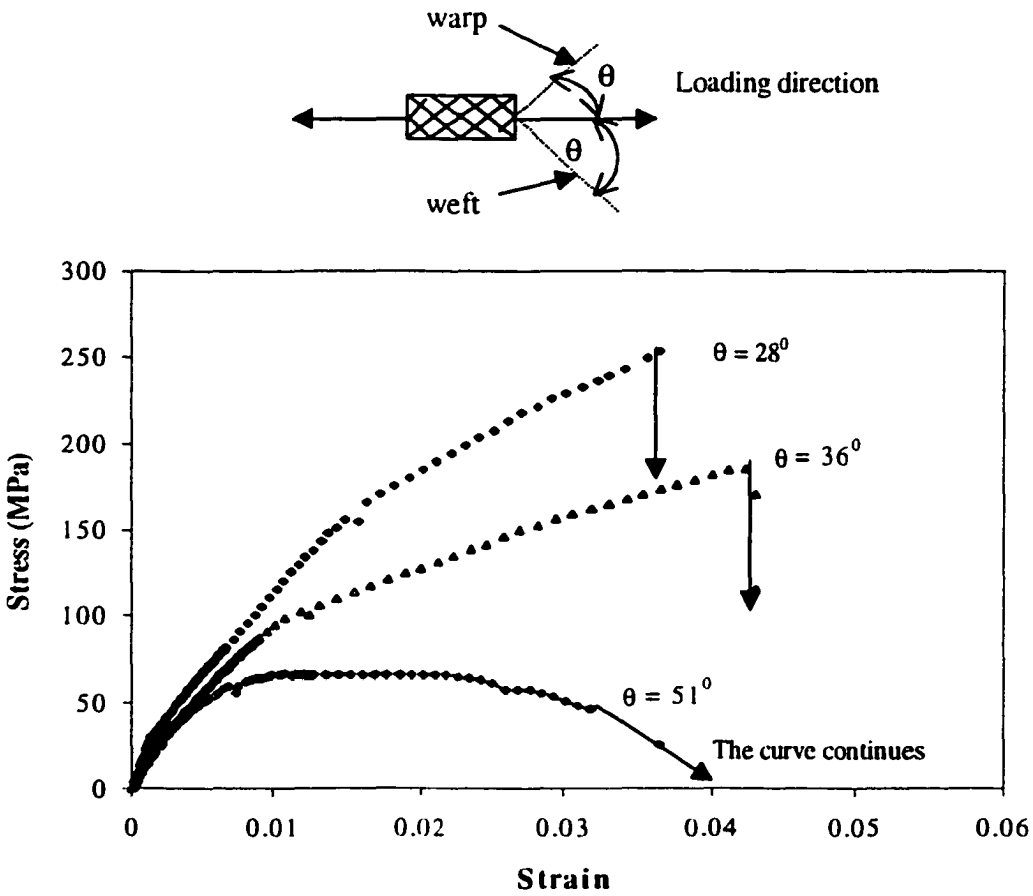

Figure 5.2 : Tensile stress-strain curves of deformed plain weave fabric composite

The different types of stress-strain curves obtained from the three typical types of deformed plain weave fabric composite are shown in Figure 5.2. We can see that these curves all have the same non-linear shape and are classified as brittle nature. However, every curve there is two distinct regions divided by a specific value of strength. At that value of strength, the curve drops suddenly in the load, and then continues increasing to ultimate strength. This may be explained by the fact that there is a unstable propagation of crack follows by an address of the crack. This value of strength seems to be a onset of damage. Furthermore, we can see in Fig. 5.2 that the strain at onset of damage will decrease when θ increases.

The strain at fracture as a function of the angle θ is shown in Figure 5.3 for tensile test. One possible explanation to this unusual behaviour is that [11] the configuration with $\theta = 45^{o}$ is the only one that has the normal stress in the fiber direction equal to the normal stress transverse to the fibers as well as having both the in-plane and interlaminar shear stress at a fairly high finite value. Such a combination could lead to gross transverse cracking and ply delamination resulting in a scissoring effect or rotation of the fibers about the longitudinal axis as the laminate continues to support a load [11].

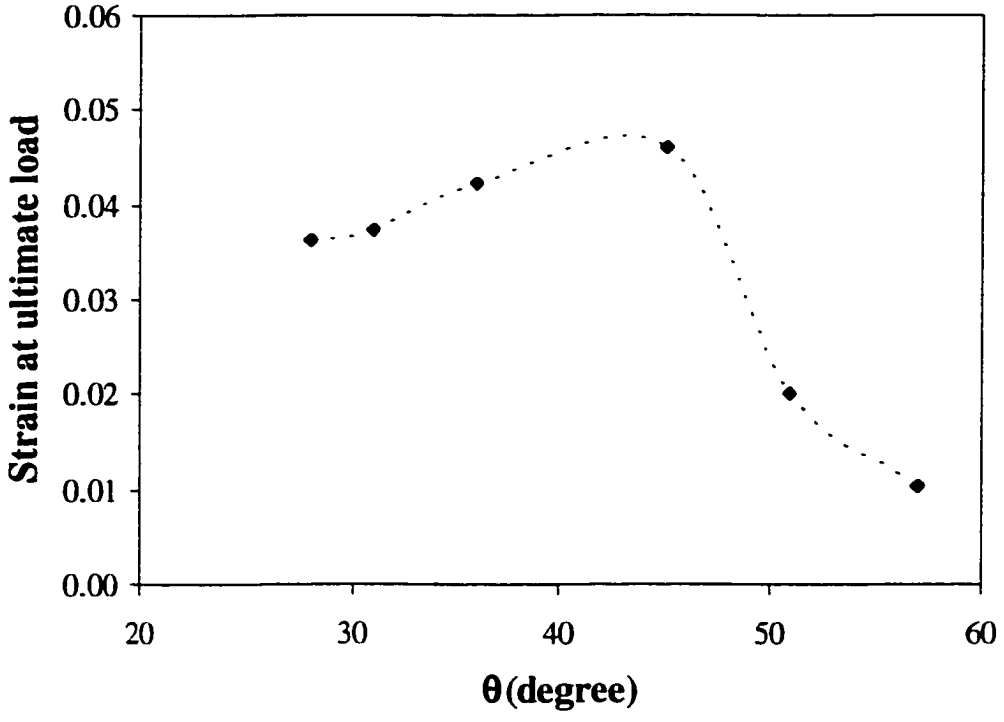

Figure 5.3 : Strain at fracture as a function of the in-plane shearing deformation angle θ

5.1.2. Failure mechanism

Figure 5.4 illustrates three basic failure modes of woven fabric composites under quasi-static loading : fiber breakage, delamination and fiber shear fracture in a kink.

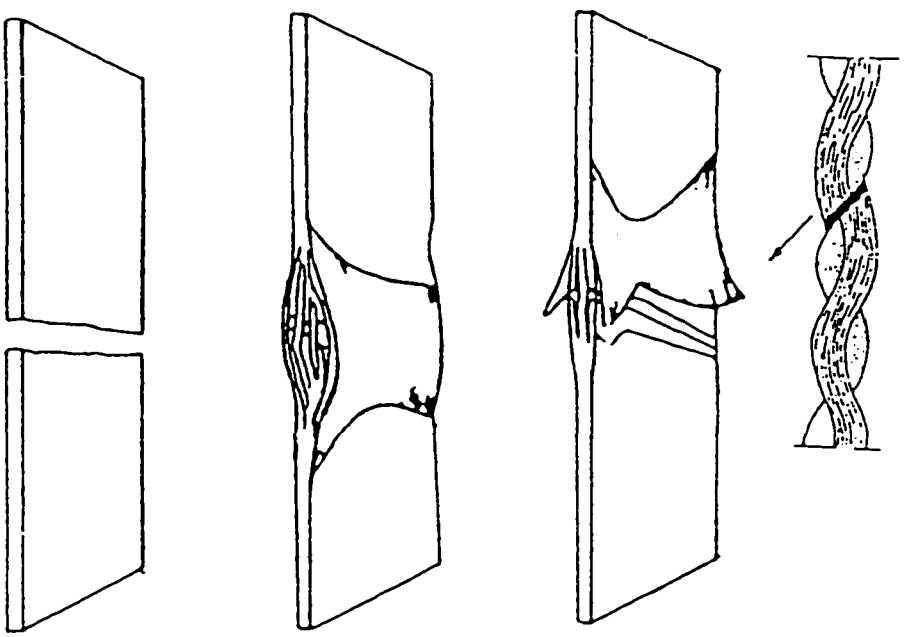

Figure 5.4 : Basic failure modes of woven fabric composite under static loading

(a) fiber breakage; (b) delamination; (c) fiber shear fracture in a kink

a) Orthogonal woven composite :

Under tensile loading, before the onset of first macroscopic failure, polyester composites exhibit debonding at the matrix interface of transverse fibers (Fig.5.5). These cracks continue propagating in the direction perpendicular to the applied stress and gradually extend the full width of the specimen. In the formation of transverse cracks, debonding (similar to delamination) between transverse and longitudinal yarns is also observed (Fig.5.6). Ultimate failure occurs when the longitudinal yarns are fractured perpendicularly to the loading direction and then pulled out from the matrix (Fig.5.7a). At this stage, the rupture take place suddenly and completely. Furthermore, the fracture surface also shows loose transverse yarns which carry an insignificant amount of load compared to the longitudinal yarns (Fig.5.7a).

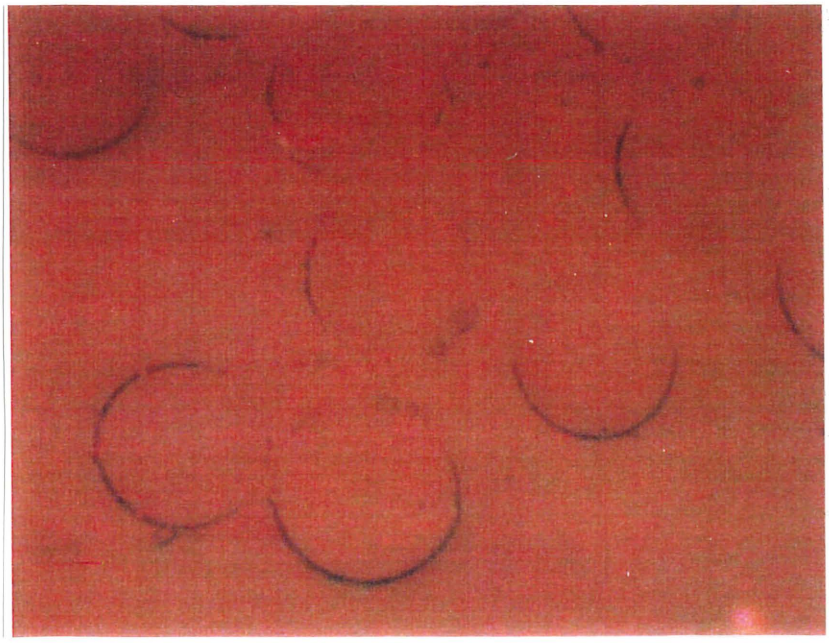

Figure 5.5 : Debonding at the interface of transverse fibers of orthogonal plain weave sample

Figure 5.6 : Debonding between weft and warp yarns
of orthogonal plain weave sample.

b) Undeformed plain weave composite with $\theta = 45^0$

Figure 5.7e and 5.8e show the photographs of tensile failure mode in specimens made of plain weave fabric and 8-harness satin composites respectively. A single fracture parallel to the fiber direction has been observed for all specimens. Specimens with $\theta = 45^0$ under tension reveal two distinct failure surfaces : one is along the warp direction and the other is along the weft direction as shown in Figure 5.7e. In the case of 8-harness satin fabric composite, it can be seen that the cross-section of specimen with $\theta = 45^0$ is significantly reduced.

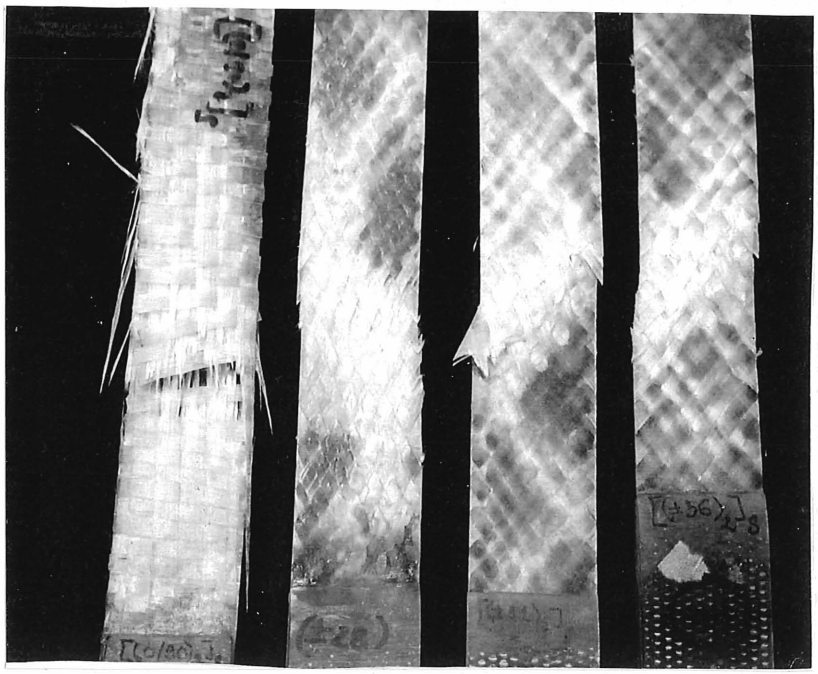

$[0/90]_s$ (a) $[\pm 28]_s$ (b) $[\pm 31]_s$ (c) $[\pm 36]_s$ (d)

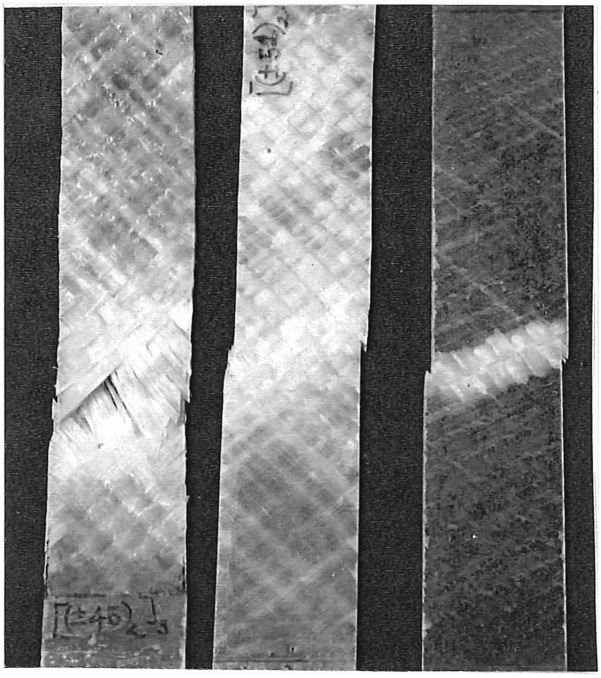

$[\pm 45]_s$ (e) $[\pm 51]_s$ (f) $[\pm 57]_s$ (g)

Figure 5.7 : Photographs of typical tensile failure of the specimens made of plain weave fabric composite.

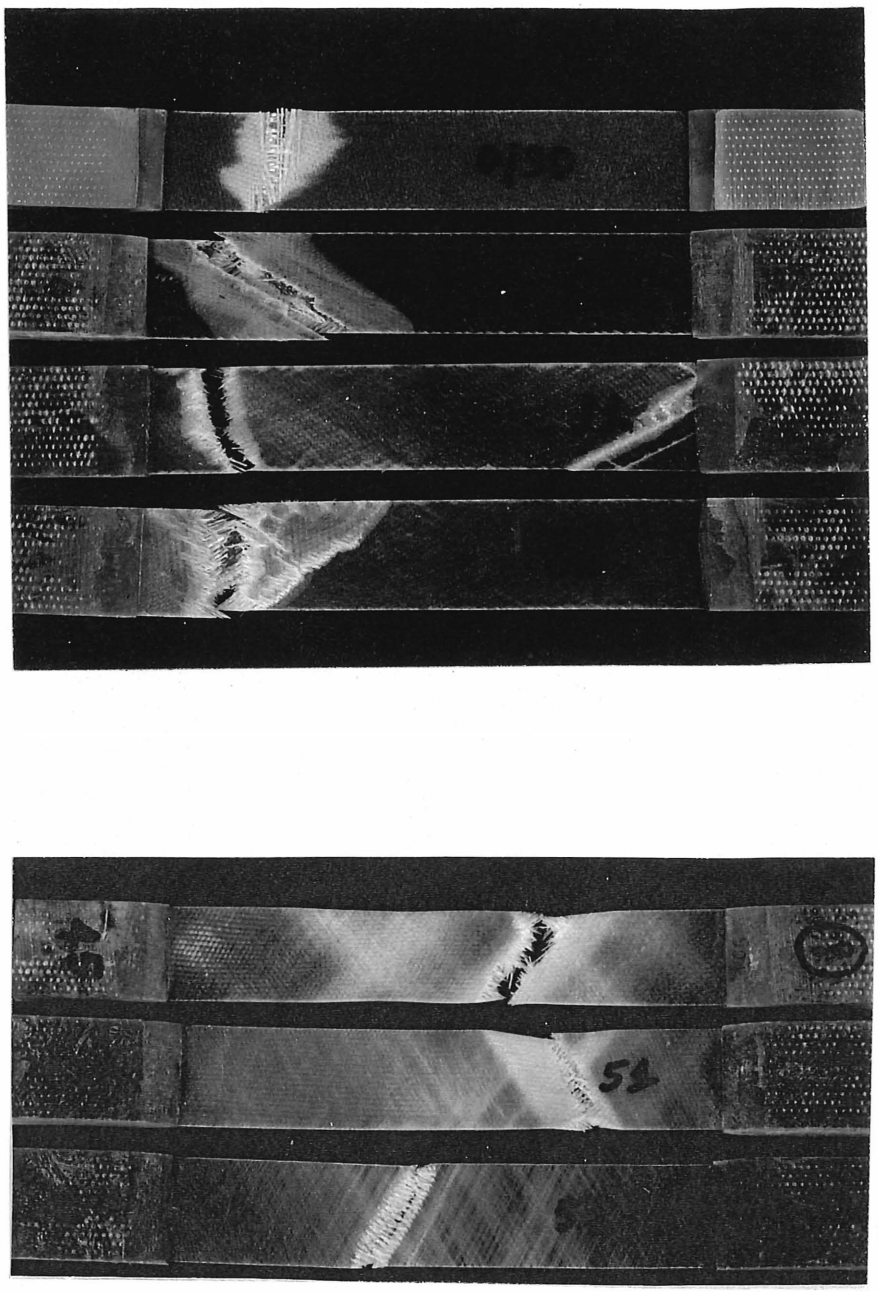

Figure 5.8 : Photographs of typical tensile failure of the specimens made of 8-harness satin fabric composite.

Tensile failures of the *[45/-45]* woven specimens involves damage accumulation in the matrix followed by fiber (yarn) failure and yarn debonding. Microscopic observation on tensile *[45/-45]* specimens indicates a network of matrix micro-cracks running along the fiber directions (Fig.5.9).

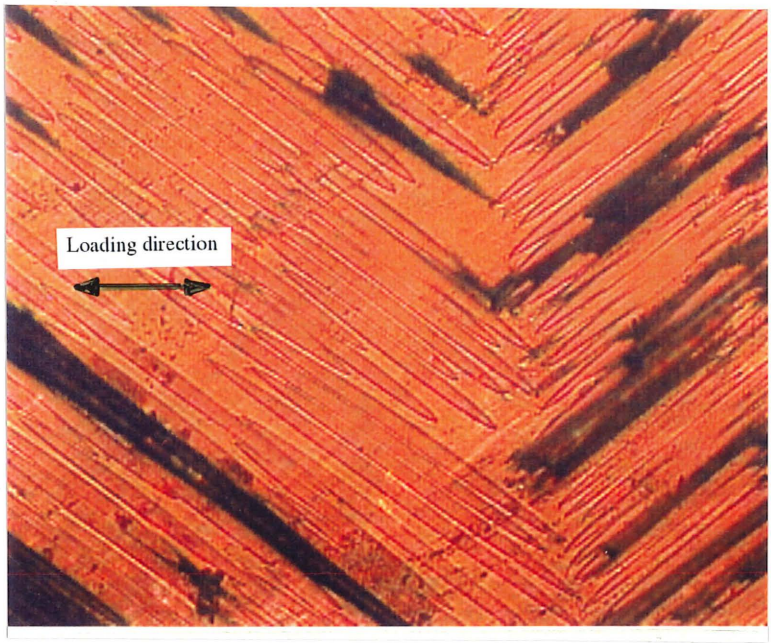

Figure 5.9 : The failure surface of *[45/-45]* specimen loaded in tension

Cracking occurs progressively in various domain, criss-crossing nearly the whole specimen. The number of cracks increases with continued elongation of the specimen. Debonding of the interlaced yarns starts at the free edge and propagates as a band along the fiber directions (Figure 5.10). Propagation of these micro-cracks in the transverse direction follows two patterns under tensile loading condition [25]. When the fibers of the facing plies run in different directions, the transverse crack propagation stops at the yarns debonding interface. When the facing plies have the same fiber direction, micro-cracks transversely

propagate through the individual laminates and delaminated interfaces, which indicates that delamination occurs during the later stages of failure. As expected the tensile failure mechanisms of the *[0/90]* specimens (loaded in 0^0 direction) are very different from those of the *[45/-45]* specimens. While damage accumulation in the form of matrix micro-cracking and propagation leads to the failure of the *[45/-45]* specimens, failure in the *[0/90]* specimens is controlled by the longitudinal yarns.

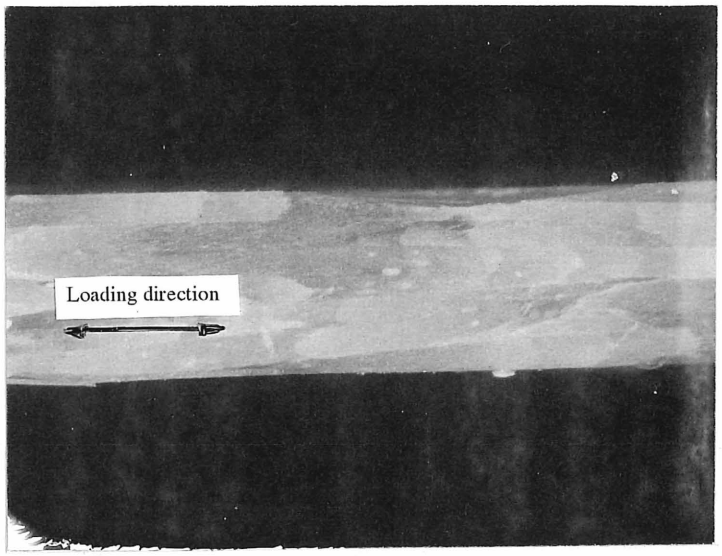

Figure 5.10 : Longitudinal cross-section at the free edge of *[45/-45]* specimen loaded in tension

c) Deformed woven composites

As in the case of laminated composites when the stress level increases, the whitening region increases. The fracture surface of this *[±28]* specimen mainly shows matrix cleavage and laceration caused by a combination of transverse tension and longitudinal shear (Fig.5.7b and Fig.5.8b). Similar failure mechanisms are also observed for the *[±31]* and *[±36]*

specimens. The failure mode of the *[±51]* and *[±57]* specimens is different from the *[±28]* and *[±45]* specimens. In the case of the *[±51]* and *[±57]* group, initial failure occurs by a major crack in fiber direction, followed by progressive parallel cracks until the ultimate failure of the specimen. This failure mode is only a local nature, the damaged region is limited to a small strip consisting of parallel cracks.

Under tensile loading, the extent of the area of damage zone in the tensile sample at fracture varies as a function of the in-plane shearing deformation angle θ and is shown in Figure 5.11. In this figure the ratio of the whitening length to gage length of the tensile sample (S%) is plotted as a function of θ. S% first increases with θ, attains a maximum values at $\theta = 45^0$ and then decreases. Similar results were also observed for 8-harness satin fabric composite.

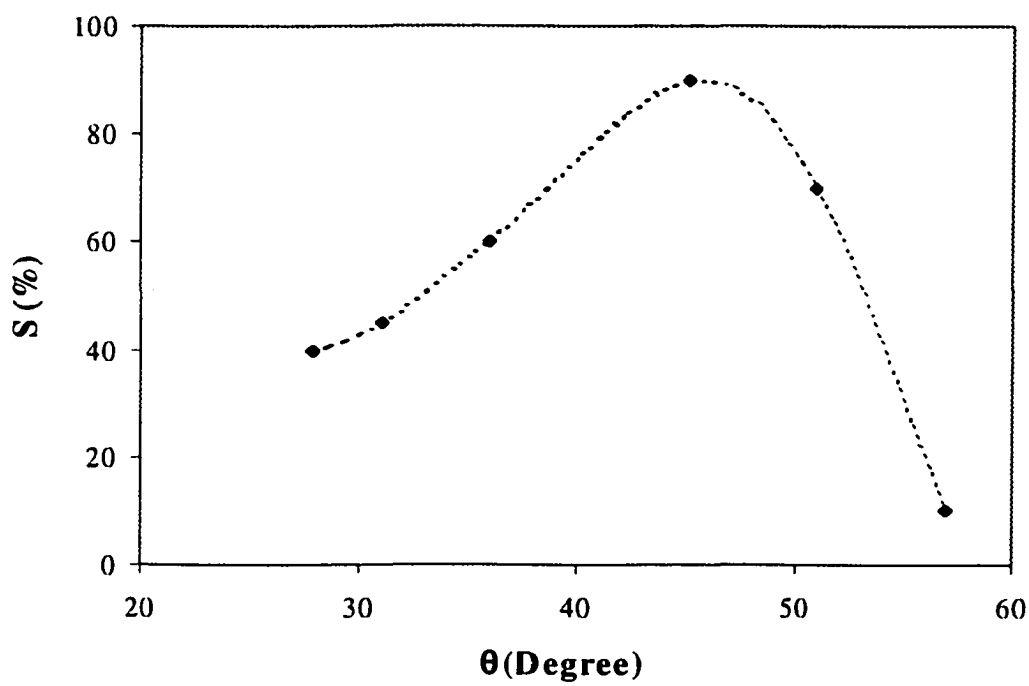

Figure 5.11 : The area of damage zone at fracture S (%) varies as a function of the in-plane shearing deformation angle θ

5.2. COMPRESSIVE TEST

5.2.1. Stress-strain curves

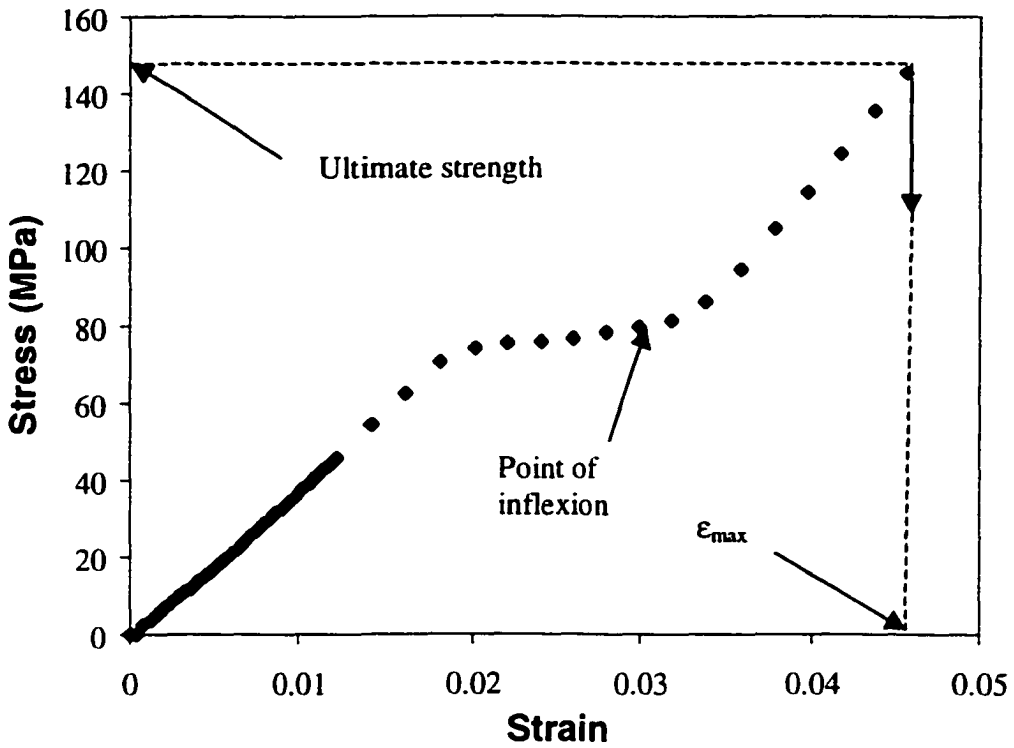

Figure 5.12a : Compressive stress-strain curve of undeformed plain weave sample (loaded in 0^0 direction)

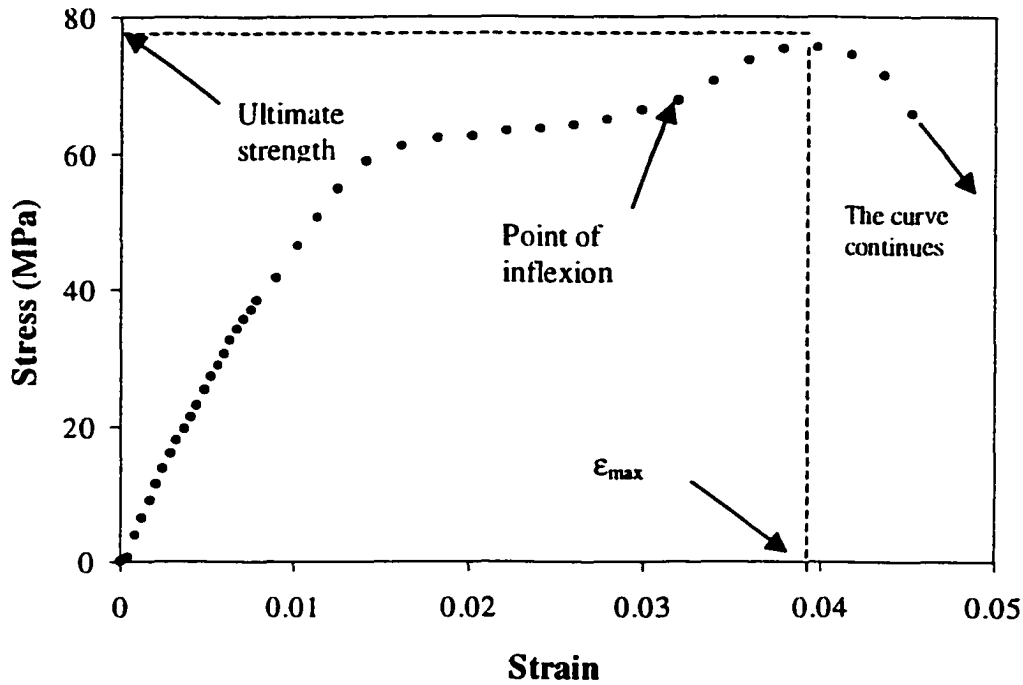

Figure 5.12b : Compressive stress-strain curve of undeformed plain weave sample with $\theta = 45^0$

In the compressive tests for undeformed plain weave samples (loaded in 0^0 and $\theta = 45^o$ directions), the bilinear behaviour is not observed and their stress-strain curves are non-linear (Fig. 5.12a and 5.12b). Both of them are complex and show peculiar behaviour. First, there is a point of inflexion in the non-linear region of these curves. After the inflexion point the composite has a hardening tendency. This may be due to the fact that in woven composite, the warp and weft yarns are woven together and are undulated. No clear fracture is observed as in the case of nonwoven composites. In woven fabric composites, it has been shown that [10] the influence of the resin is most apparent in the regions where the fiber weave creates resin-rich areas. The intersection of four yarns formed an interstitial region where the resin was nearly as thick as the ply itself. The interstitial region of the surface contains a chunk of resin

with fiber imprints, implicating that the crack jumped from one ply interface through the resin layer between the plies to the neighbouring ply interface.

The ultimate compressive strength of the [0/90] plain weave specimen is found to be 50 per cent lower than their ultimate tensile strength. This value of ultimate compressive strength was used to determine the longitudinal compression strength coefficient (X') as showed in the previous chapter.

The ultimate compressive strength of the [45/-45] plain weave specimen is equivalent to their ultimate tensile strength. On the other hand, the ultimate compressive strength of the [45/-45] 8-harness satin specimen is 15 per cent higher than their ultimate tensile strength. The results suggest that shear failure is dominant in both tensile and compressive tests.

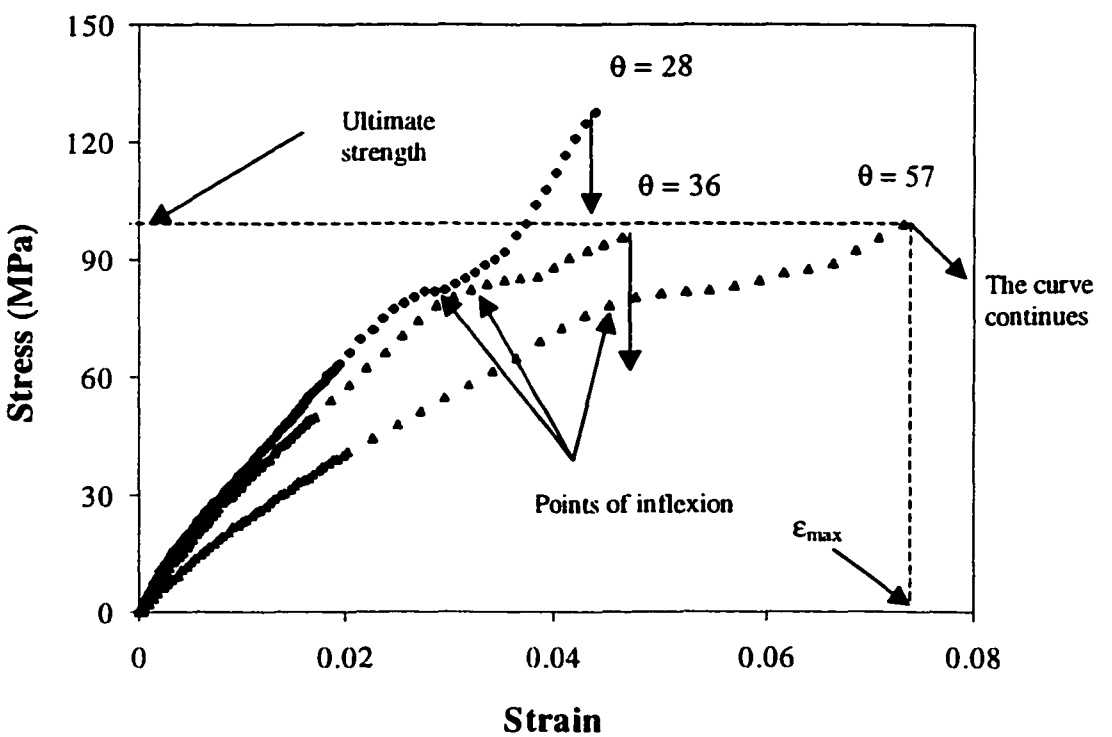

Figure 5.13 : Compressive stress-strain curves of deformed plain weave fabric composite

Three typical stress-strain curves of the other deformed plain weave samples under compressive loading are shown in Figure 5.13. They also present a non-linear shape as for laminated composites and also have peculiar behaviour. The points of inflexion are also found on these curves. In compression the *[±45]* specimen no longer exhibits the largest strain (at maximum load) as in the case of tension.

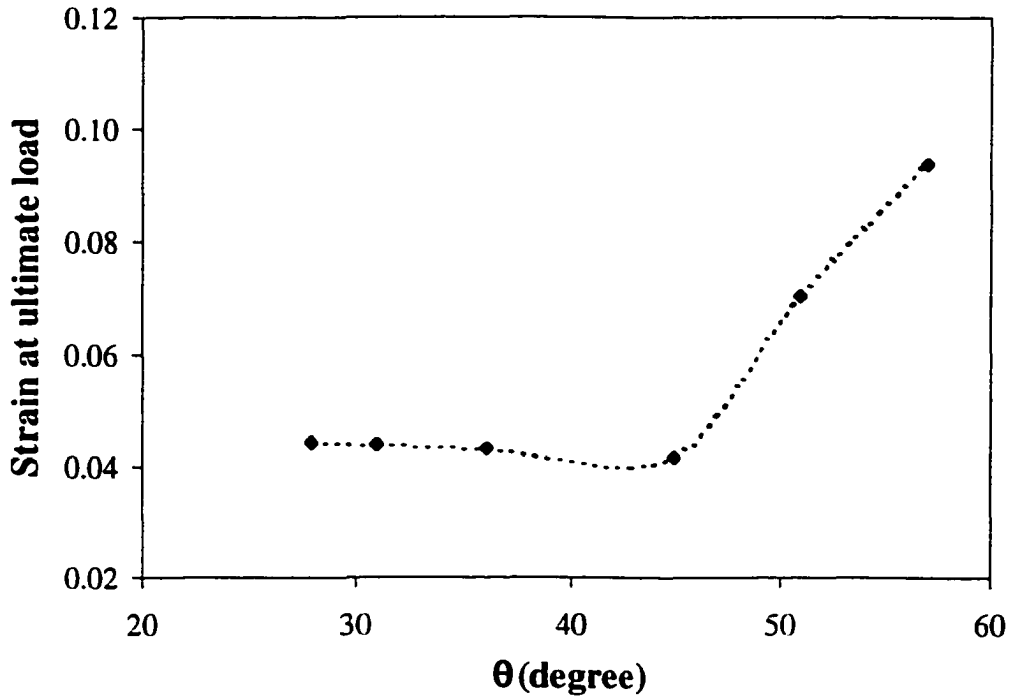

Figure 5.14 : Strain at fracture as a function of the in-plane shearing deformation angle θ under compressive loading

Figure 5.14 shows the strain at fracture (maximum load) versus the angle θ for deformed plain weave fabric composite under compressive loading. It can be seen that the strain at fracture of the specimen with $\theta = 45^{o}$ seems to be minimum. In 8-harness satin fabric, the same tendency is also observed (as in the case of plain weave fabric, Fig. 5.14).

5.2.2. Failure mechanism

(a)

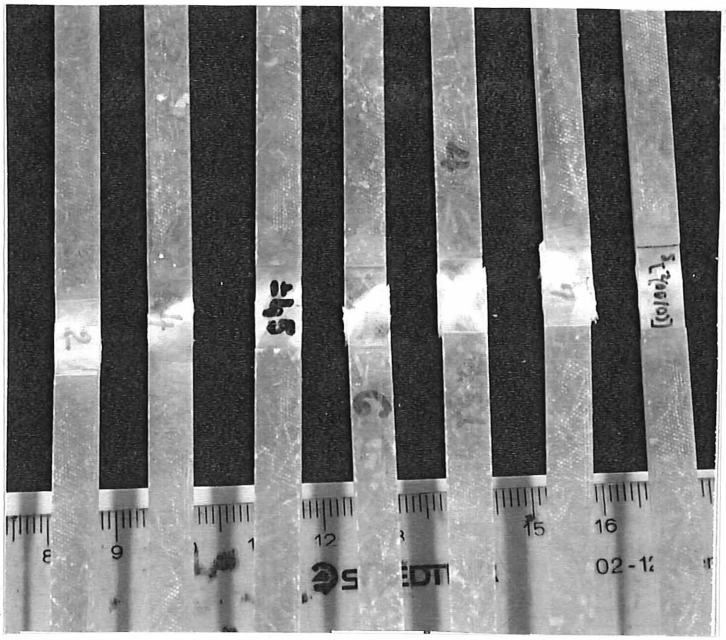

$[\pm57]_s$ (g) $[\pm51]_s$ (f) $[\pm45]_s$ (e) $[\pm36]_s$ (d) $[\pm31]_s$ (c) $[\pm28]_s$ (b) $[0/90]_s$ (a)

(b)

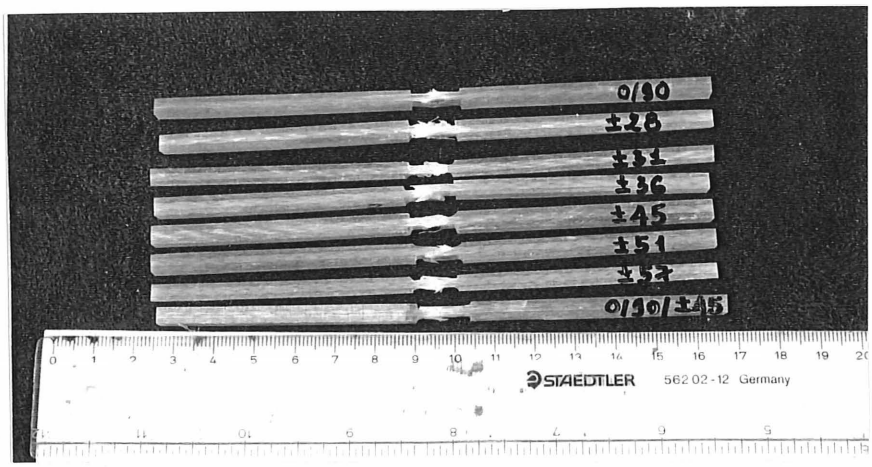

Figure 5.15 : Photographs of the typical compressive failures of the specimens made of plain weave fabric composite

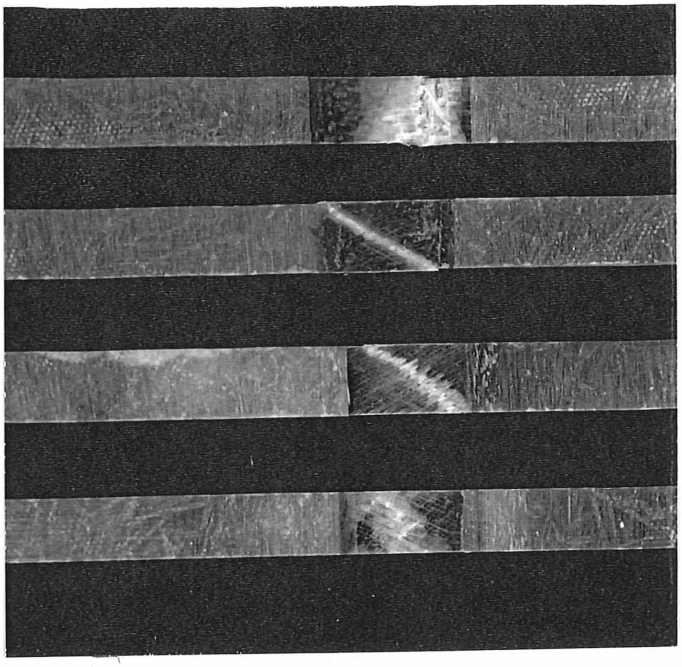

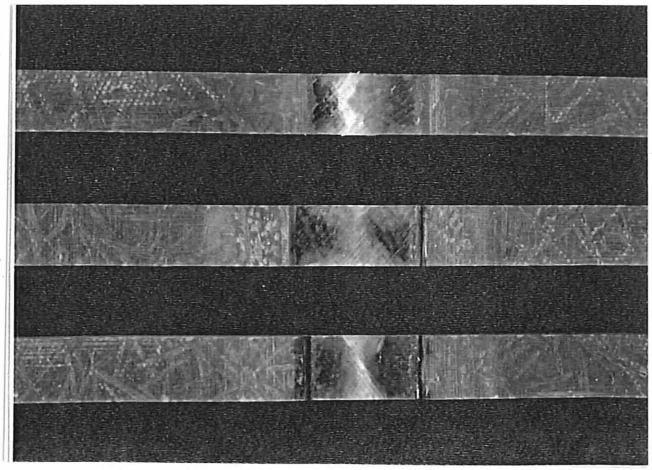

Figure 5.16 : Photographs of typical compressive failure of the specimens made of 8-harness satin fabric composite.

Figure 5.15 and 5.16 show failure modes and damage patterns in compressive specimens for plain weave and 8-harness satin fabric composites. In those cases, we can see that the failure and damage patterns are similar for the two composites (plain weave and 8-harness satin). In Fig. 5.15b, there is a separation between warp and weft yarns and also delamination between the distinct layers. For all specimens, debonding and delamination between the distinct layers will propagate through the thickness and across the width of the specimen along the warp or weft fiber direction.

Under compressive loading condition, the *[0/90]* woven specimens fail due to transverse shear. The fracture surface was also observed, it makes an angle about 20-30 degrees to the loading direction as showing in Figure 5.17a. Compressive failure of the longitudinal yarns is due to fibre breakage and kinking of the fibers in the out-of-plane direction as 5-harness satin fabric [25].

Figure 5.17 (a) : Failure surface of orthogonal plain weave specimen loaded in compression

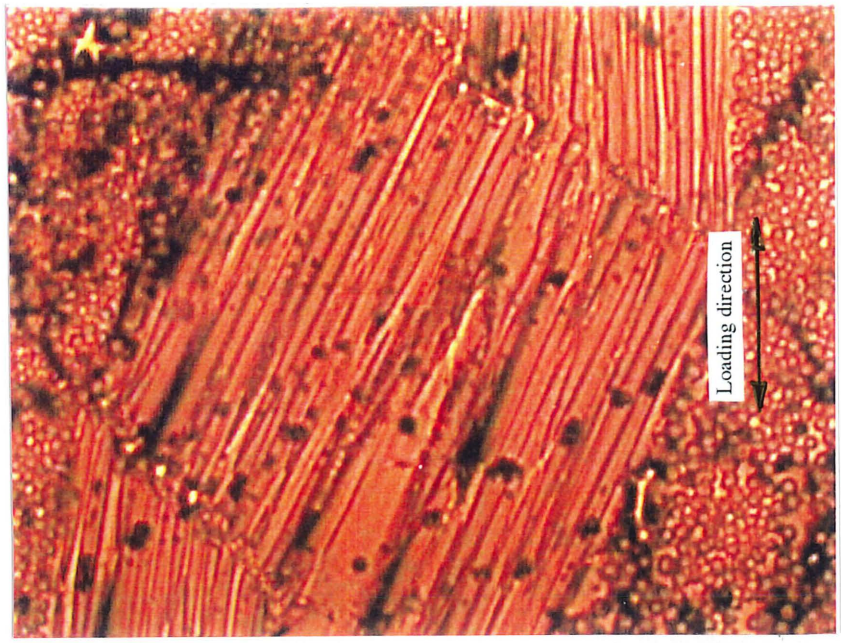

Figure 5.17 (b) : Micrograph of longitudinal cross-section of orthogonal plain weave specimen loaded in compression

Failure in the *[45/-45]* woven specimen was always centred in the gage length of the specimen, whereas fracture of the *[45/-45]* specimen made from unidirectional plies was generally located nearer the tab ends [3]. In the case of woven composite, damage accumulation in the matrix is followed by buckling of yarns in the transverse direction (Figure 5.18). Buckling of the yarns is promoted at the interlace regions, which the fibers are inclined in the out-of-plane direction. In general, the failed *[45/-45]* specimen showed less fibre fracture than in *[0/90]* specimen. Transverse debonding is however pronounced in these samples (Fig.5.19).

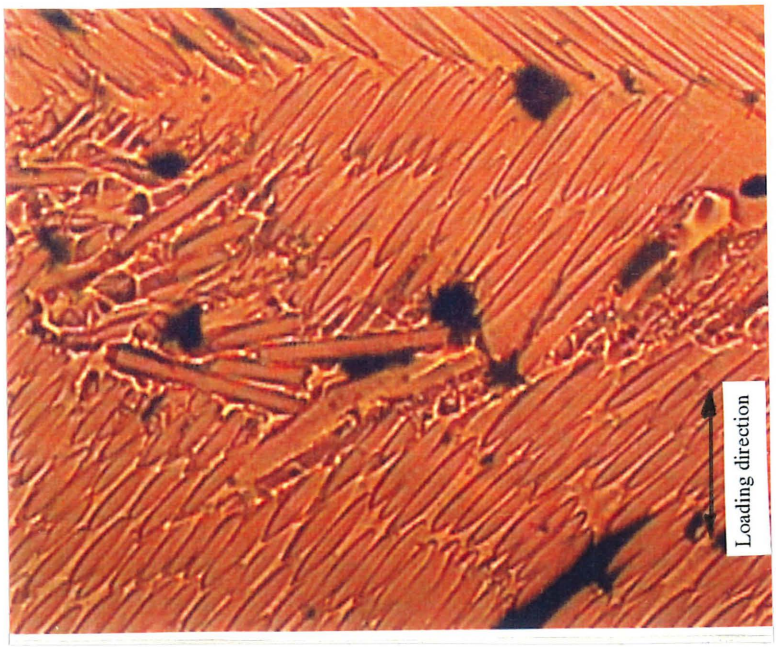

Figure 5.18 : Micrograph of longitudinal cross-section of [±45] specimen loaded in compression

Figure 5.19 : Cross-section of [±45] specimen loaded in compression

Appearance of damage of deformed woven fabric composites under compressive loading condition is similar in angle-ply composite made of unidirectional layers. The layer showing broken fiber ends is considered to have failed immediately after the other layer. Thus, the layer shows the fiber surface is primarily responsible for failure [27]. Whole tow breaks, laceration and cleavage indicated that all three stress components appear to play a significant role in the failure of these specimens (Fig.5.15 and Fig.5.16).

5.3. DETERMINATION OF THE FAILURE ENVELOPES OF DEFORMED WOVEN FABRIC COMPOSITES

5.3.1. Tensile test

5.3.1.1. Onset of damage

The onset of ply failure and the ultimate strength of the laminates were determined using the composite laminate design software Genlam [47]. In the calculation, various strength coefficients determined from the above tests (Table 4.3) were examined. Both the maximum strain and the quadratic criteria were applied. The onset of ply failure of the plain weave fabric composite was determined from the points of sudden drop in the load in the stress-strain curves (Table 5.1).

Table 5.1 : Onset of damage in tensile tests of deformed plain weave fabric composite

Types	Number of specimens	Standard deviation	Onset of damage (MPa)
$[(-28/+28)_n]_s$	6	4.12	156.65
$[(-31/+31)_n]_s$	6	3.18	90.69
$[(-36/+36)_n]_s$	7	4.16	92.03
$[(-51/+51)_n]_s$	5	2.60	58.19
$[(-57/+57)_n]_s$	5	2.12	47.27

5.3.1.2. Ultimate tensile strengths

The ultimate tensile strengths of woven fabric composites are mainly the value of obtained maximum stresses in the stress-strain curves are shown in Tables 5.2 and 5.3.

Table 5.2 : Ultimate tensile strength of deformed plain weave fabric composite

Types	Number of specimens	Standard deviation	Ultimate strength (MPa)
$[(0/90)_n]_s$	8	5.190	291.40
$[(-28/+28)_n]_s$	6	5.070	235.18
$[(-31/+31)_n]_s$	6	8.320	214.57
$[(-36/+36)_n]_s$	7	3.610	192.69
$[(-45/+45)_n]_s$	6	3.100	80.97
$[(-51/+51)_n]_s$	5	2.520	59.44
$[(-57/+57)_n]_s$	5	1.480	48.32

Table 5.3 : Ultimate tensile strength of deformed 8-harness satin fabric composite

Types	Number of specimens	Standard deviation	Ultimate strength (MPa)
$[(0/90)_n]_s$	5	7.060	352.73
$[(-28/+28)_n]_s$	5	3.460	306.16
$[(-31/+31)_n]_s$	5	4.210	207.13
$[(-36/+36)_n]_s$	5	3.550	177.79
$[(-45/+45)_n]_s$	5	2.500	76.70
$[(-51/+51)_n]_s$	5	2.740	53.60
$[(-57/+57)_n]_s$	5	1.040	43.51

The ultimate predicted strength was determined using the procedure proposed in [47], as discussed above, to simulate the gradual degradation of the laminate due to the failure of successive plies with increasing loading. In general, the results showed that the quadratic criterion provides a better prediction at both the onset of damage and at the ultimate failure of the woven fabric composites so that only predictions from the quadratic criterion are presented.

The ultimate tensile strengths versus angle θ for plain weave fabric composite were determined with *(DF)* = 0.1 and 0.2 have been shown in the Table 5.4. The results clearly show that using a value of *(DF)* = 0.1 for polyester/glass composite is reasonable.

Table 5.4 : Ultimate tensile strengths of deformed plain weave fabric composites which were determined using *(DF)* of 0.1 and 0.2.

θ (degree)	15	25	35	45	55	65
***DF* = 0.1**	566.0	375.0	182.0	87.2	48.0	32.5
***DF* = 0.2**	547.0	348.0	169.0	82.9	46.8	32.3

5.3.1.3. Prediction of the major Poisson' s ratio values

The major Poisson' s ratio values of the deformed woven fabric composites are shown in Figures 5.20 and 5.21 as a function of the deformation angle. Predictions are based on the sub-plies model using the mechanical properties determined experimentally from woven fabric and unidirectional samples. These results show a good agreement between experimental data and the results predicted by the sub-plies model with properties measured on the woven samples.

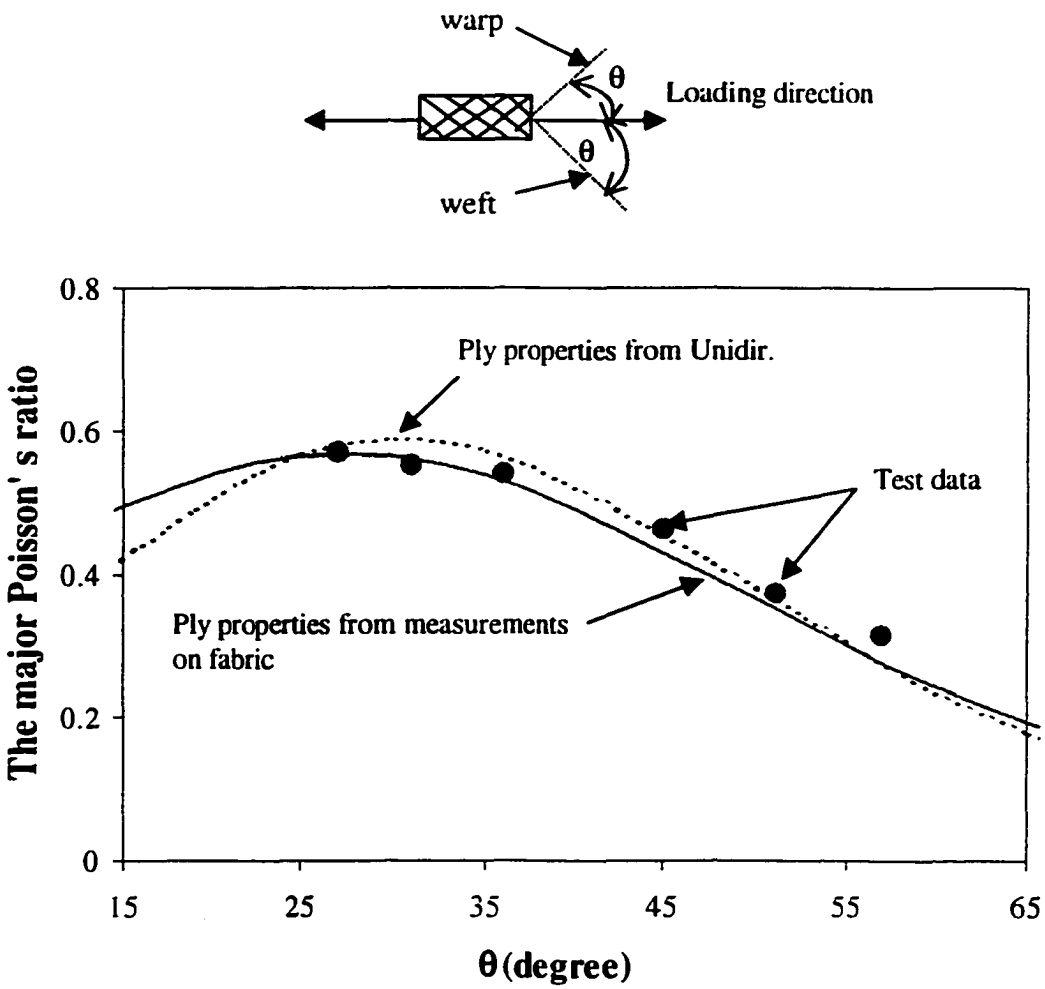

Figure 5.20 : Variation of the major Poisson' s ratio as a function of deformation angle of unidirectional and plain weave fabric composites.

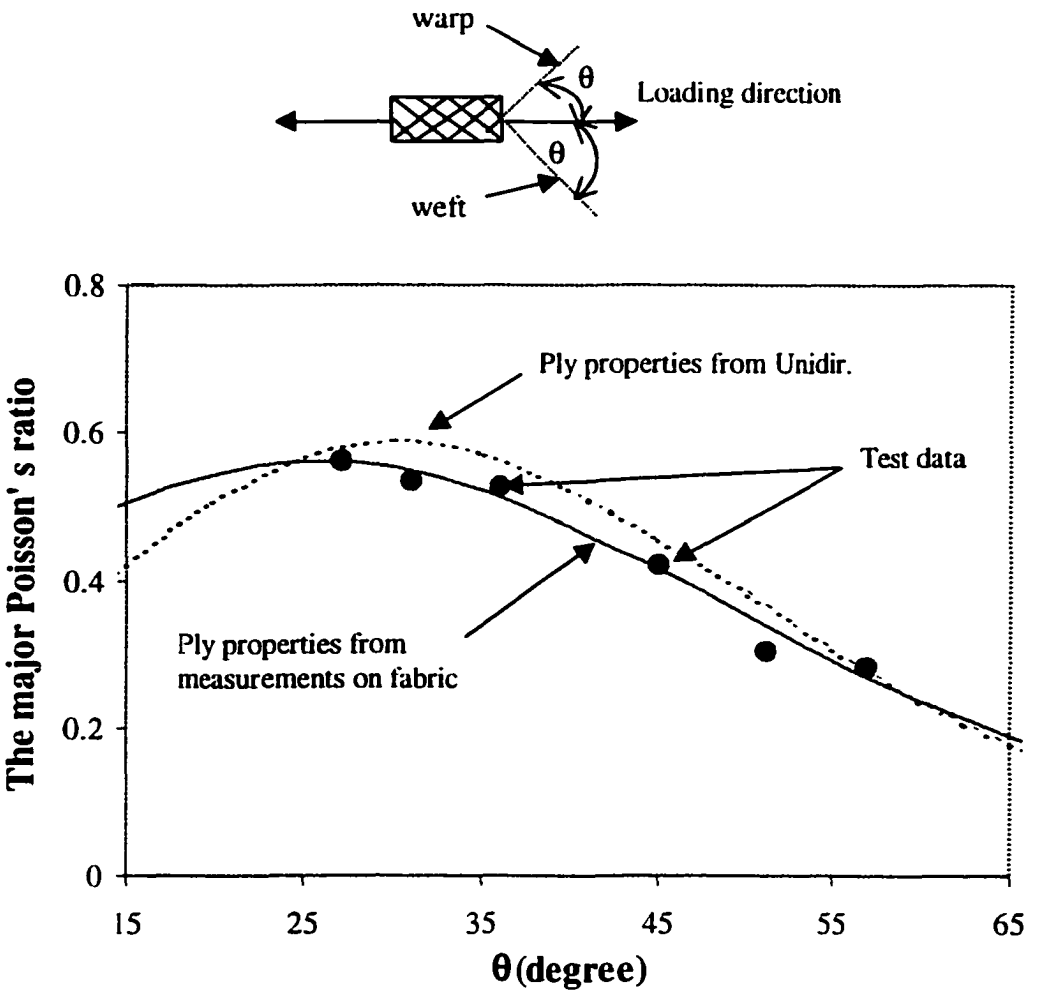

Figure 5.21 : Variation of the major Poisson' s ratio as a function of deformation angle of unidirectional and 8-harness satin fabric composites.

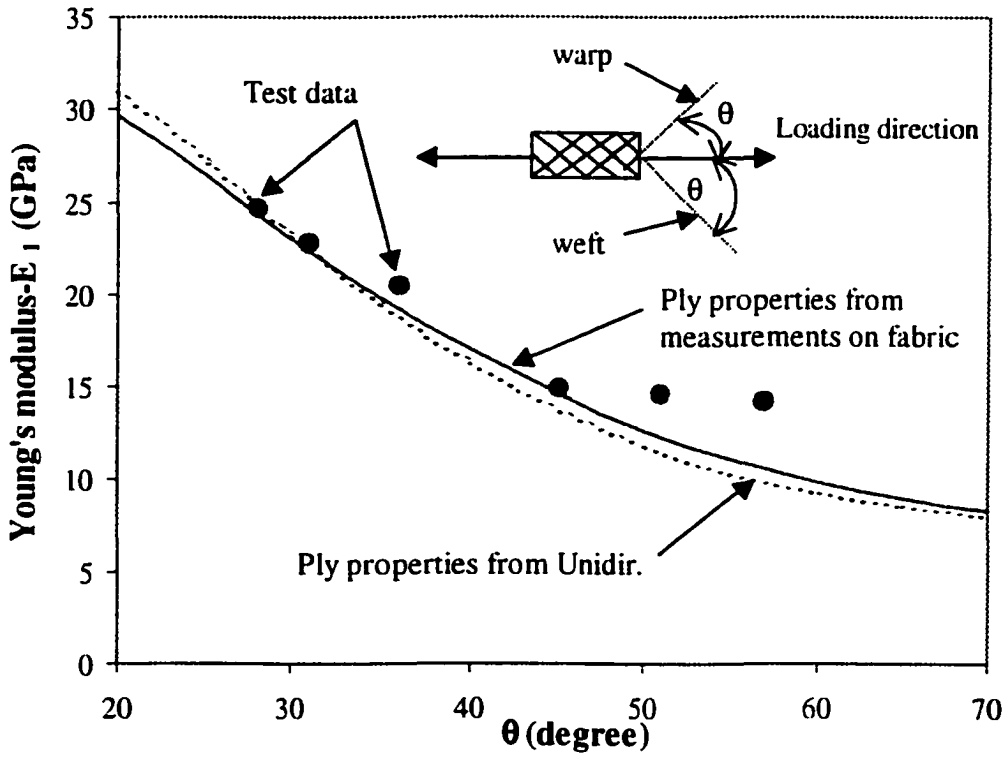

Figure 5.22 : Variation of the Young' s modulus of the deformed composites as a function of θ for the plain weave fabric composite

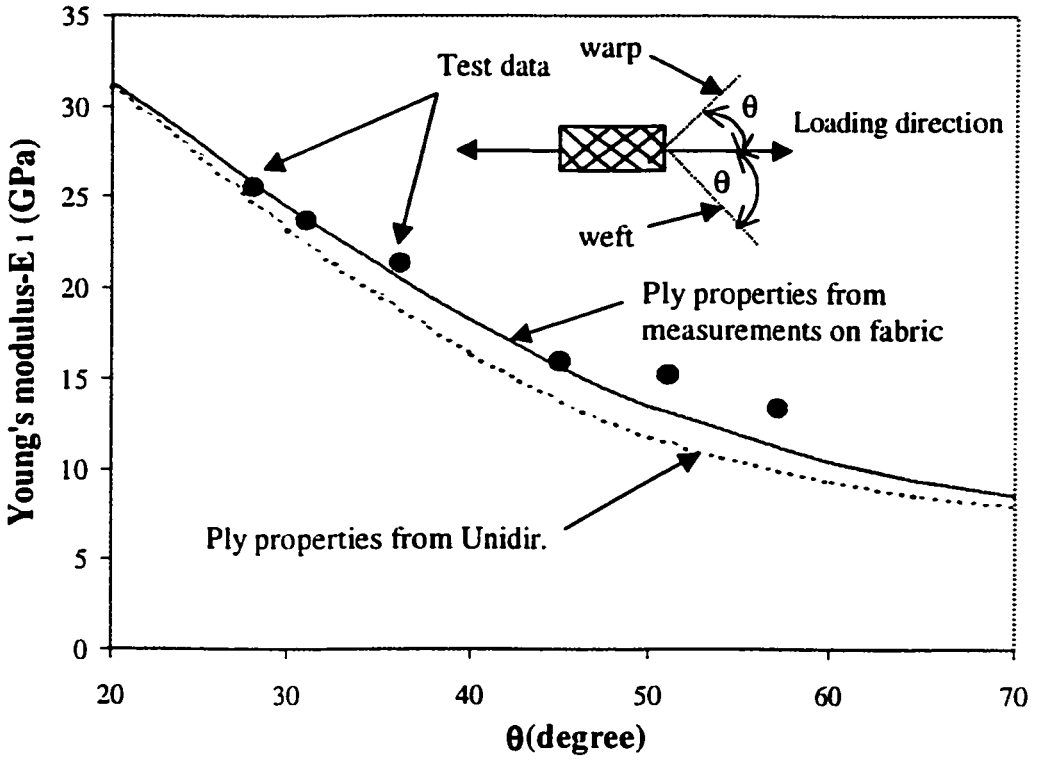

Figure 5.23 : Variation of the Young' s modulus of the deformed composites as a function of θ for the 8-harness satin fabric composite.

5.3.1.4. Prediction of the Young' s modulus

Figures 5.22 and 5.23 show the variation of the Young' s modulus of the deformed composites as a function of θ for the plain weave and the 8-harness satin fabrics, respectively. It can be seen that prediction based on the sub-plies model is in good agreement with experimental measurements. The proposed sub-plies model allows relatively accurate prediction of the mechanical properties of deformed fabrics with various weave patterns. For comparison purpose, predictions based on the properties measured on the unidirectional composite are shown. In calculation, we know that the shear modulus affects strongly the Young' s modulus of angle laminates especially, when value of angle θ increases. Because the values of shear modulus of woven fabric composites are higher than those of unidirectional composite (Table 4.2), the obtained prediction values of the Young' s modulus for woven fabric composites are reasonably higher.

5.3.1.5. Failure envelopes of deformed woven fabric composites

Figures 5.24, 5.25 and 5.26 present the comparison between the prediction using the sub-plies model and experimental measurements of tensile strength of deformed woven fabric composites. The onset of damage (first cracking) and ultimate tensile strengths of the woven laminates are shown as a function of the deformed angle θ. In all cases, the results of experimental measurements are in relatively good agreement with predictions by the sub-plies model.

5.3.2. Compressive test

The comparison of the ultimate compressive strengths of the deformed fabric composite, shown in Table 5.5 and 5.6 with theoretical predictions in Figures 5.27 and 5.28 shows relatively good agreement between prediction and experimental measurement.

Table 5.5 : Ultimate compressive strength of deformed plain weave fabric composite.

Types	Number of specimens	Standard deviation	Compressive strength (MPa)
$[(0/90)_n]_s$	8	5.10	144.50
$[(-28/+28)_n]_s$	8	4.19	123.09
$[(-31/+31)_n]_s$	7	3.86	111.46
$[(-36/+36)_n]_s$	6	2.09	102.44
$[(-45/+45)_n]_s$	6	4.13	83.09
$[(-51/+51)_n]_s$	6	4.87	89.10
$[(-57/+57)_n]_s$	6	4.44	91.57

Table 5.6 : Ultimate compressive strength of deformed 8-harness satin fabric composite.

Types	Number of specimens	Standard deviation	Compressive strength (MPa)
$[(0/90)_n]_s$	5	5.15	181.77
$[(-28/+28)_n]_s$	5	6.69	145.30
$[(-31/+31)_n]_s$	5	4.64	138.05
$[(-36/+36)_n]_s$	5	15.27	113.22
$[(-45/+45)_n]_s$	5	2.28	90.20
$[(-51/+51)_n]_s$	5	4.73	93.72
$[(-57/+57)_n]_s$	5	9.15	95.65

5.3.3. Discussion

From these results, it can be seen that when the fiber undulation effect is considered (when the strength coefficients determined from the coupons made of the woven composite are used) the theoretical prediction is relatively close to that obtained by using the strength coefficients measured from unidirectional samples. Only for the case of first cracking (Fig. 5.24), with the angle θ below 80°, that the strength coefficients including fiber undulation effect provide a better result. This is rather surprising, since fiber undulation in the woven composite results significantly lower values of X. This might be explained by the fact that in these uniaxial tensile and compressive tests, X does not play a predominant role in the strength of the composite in these test directions. The effects of fiber undulation on the strength of deformed woven fabric composites can be seen from the failure envelops shown in Figures 5.29 to 5.34. The failure envelops of the woven composites were computed for the angles between the warp and the weft threads of 62°, 114°, and 90°. The results suggest that the effect of fiber undulation would be more important in the region of biaxial loading and specially in the case of plain weave fabric composite this effect is more obvious. In the case of tensile and compressive uniaxial strengths, the two envelops (Figures 5.29 and 5.30) which are calculated from the strength coefficients measured from plain weave fabric composite and unidirectional samples almost coincide. This result is also seen more clearly for the case of 8-harness satin fabric (Figures 5.32 and 5.33). This explains the lesser effect of fiber undulation shown in Figures 5.24 to 5.28.

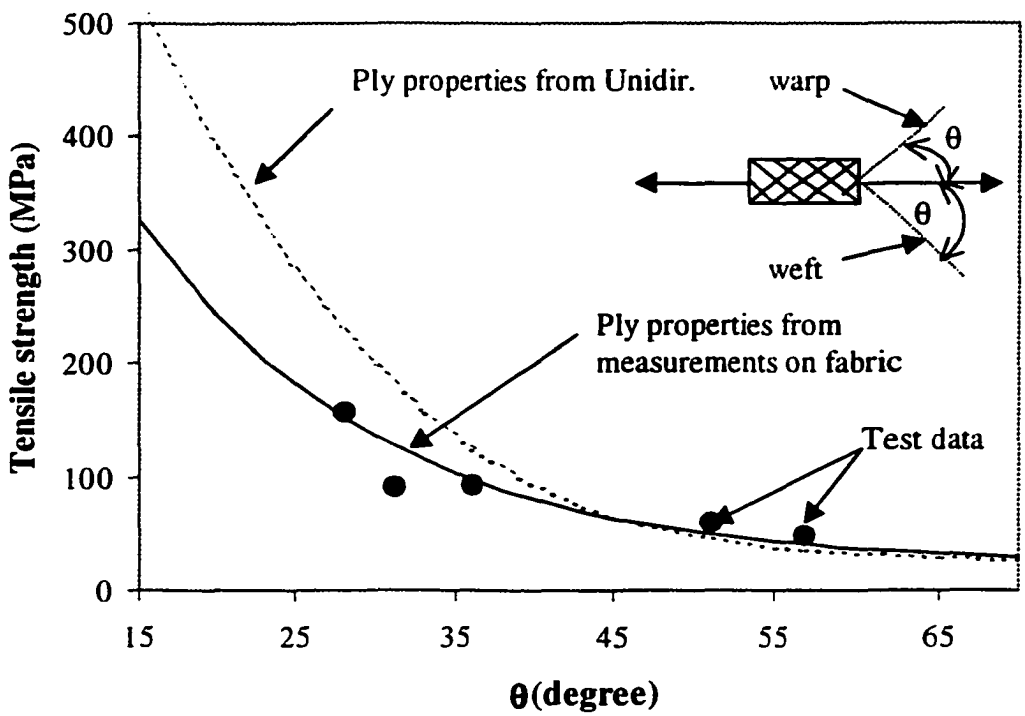

Figure 5.24 : Onset of damage in tensile plain weave samples as function of angle θ

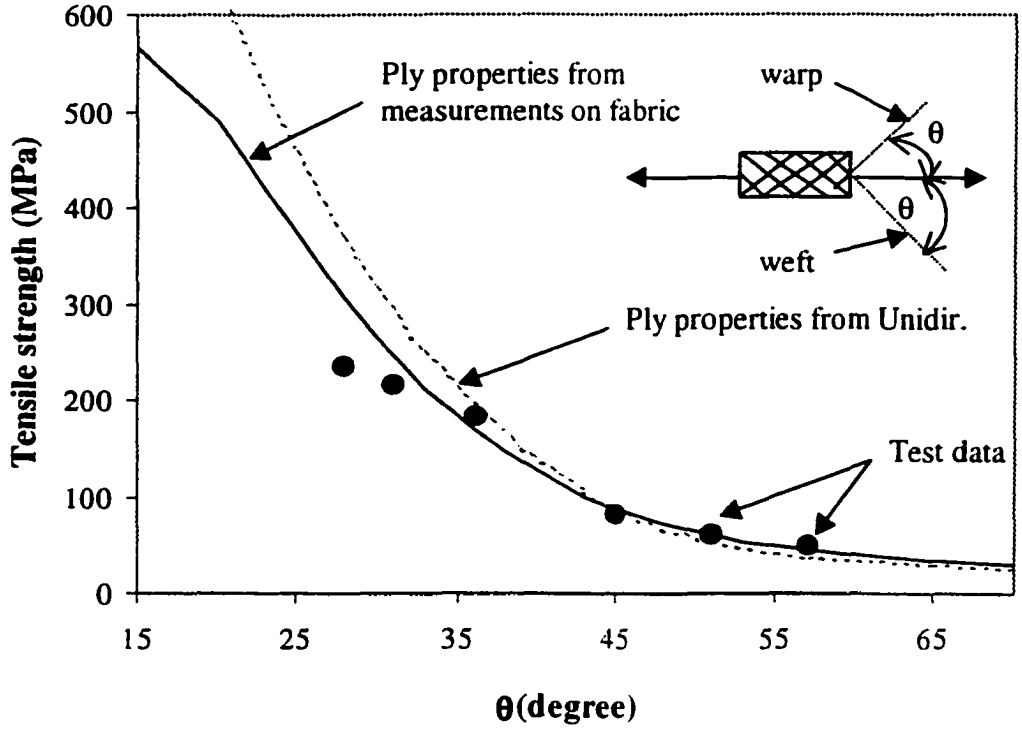

Figure 5.25 : Ultimate tensile strength for plain weave fabric composite

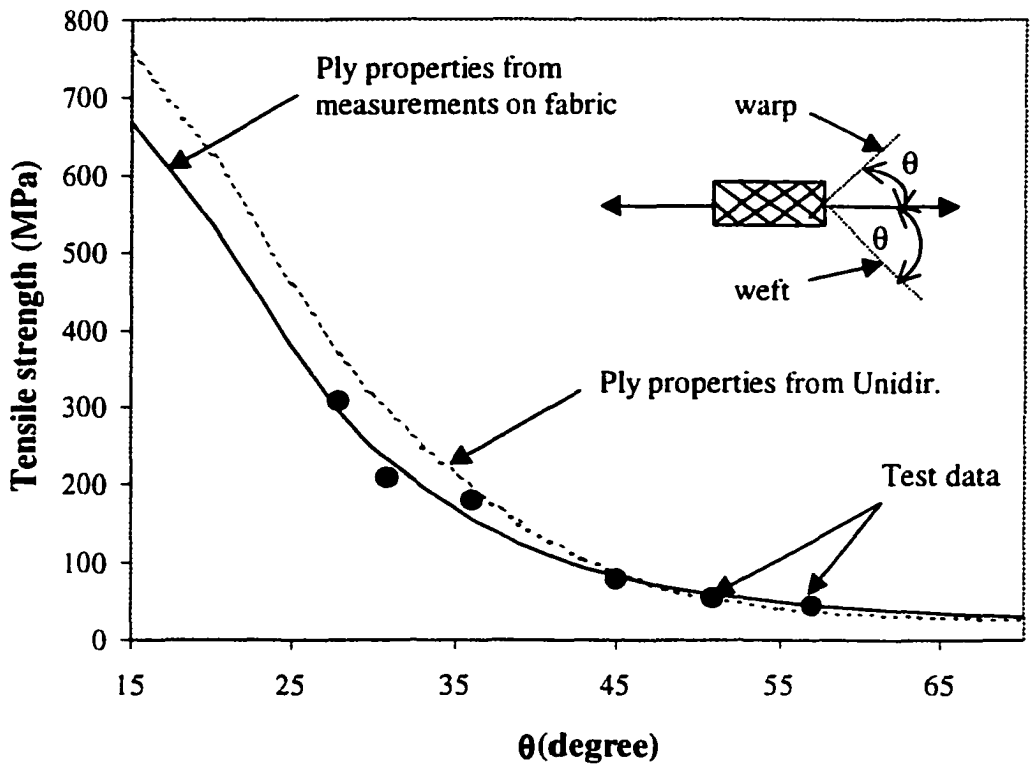

Figure 5.26 : Ultimate tensile strength for 8-harness satin fabric composite

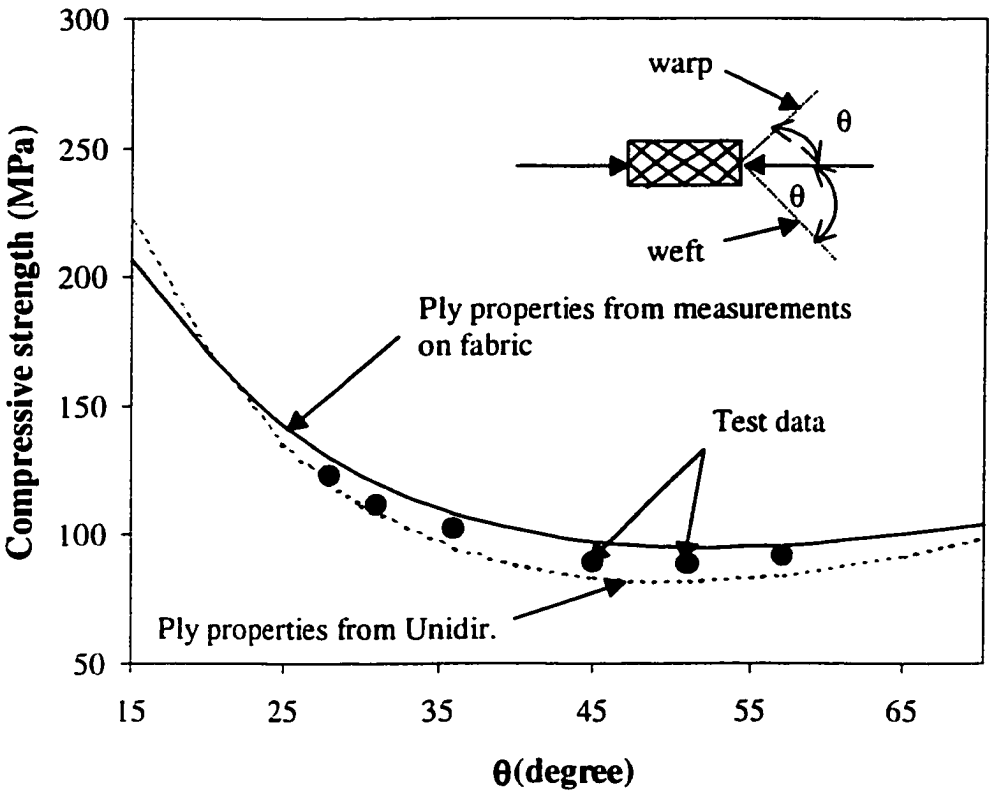

Figure 5.27 : Ultimate compressive strength for plain weave fabric composite.

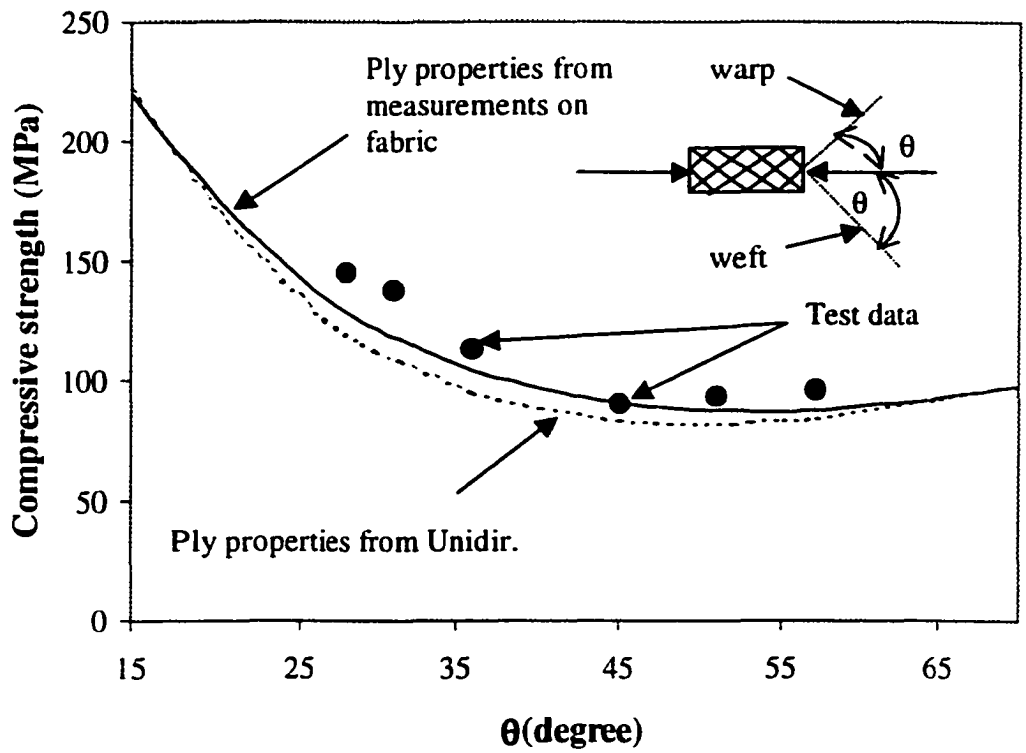

Figure 5.28 : Ultimate compressive strength for 8-harness satin fabric composite.

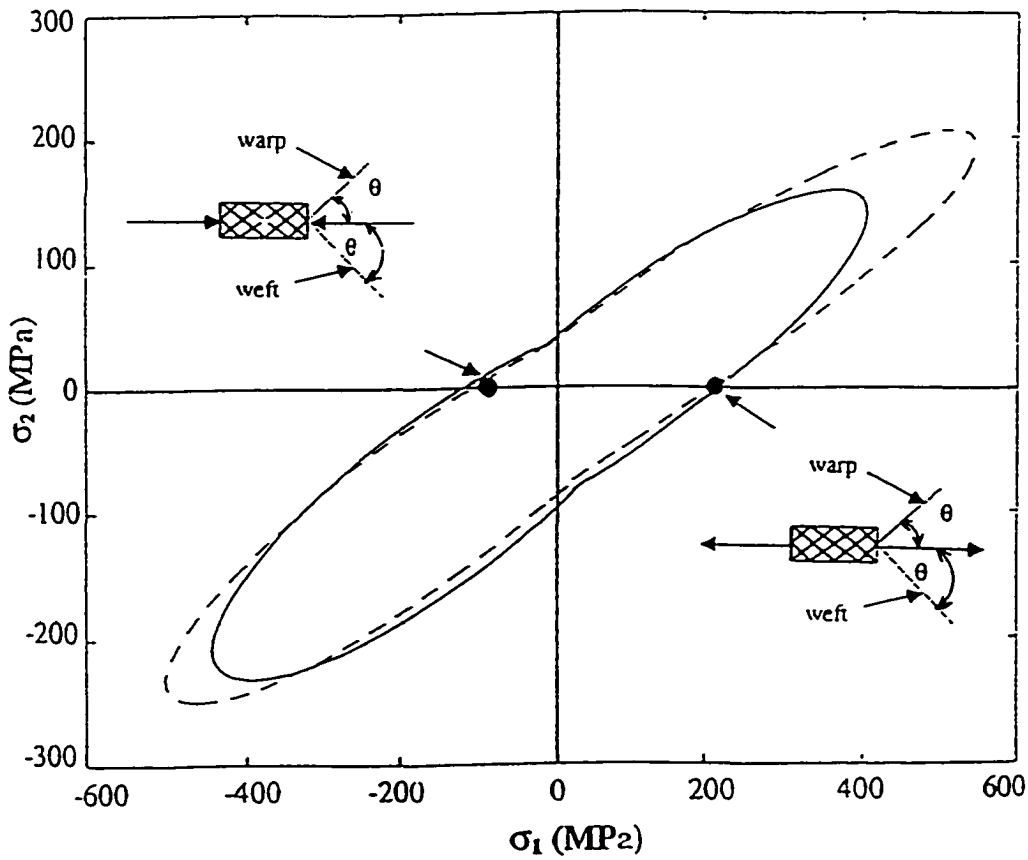

Figure 5.29 : In-plane ultimate strength envelopes of deformed plain-weave composite with $\theta = 31^0$ ($\sigma_{16} = 0$)

— Quadratic criterion using ply properties from measurement on fabric composite;

--- Quadratic criterion using ply properties from unidirectional composite;

● Experimental data.

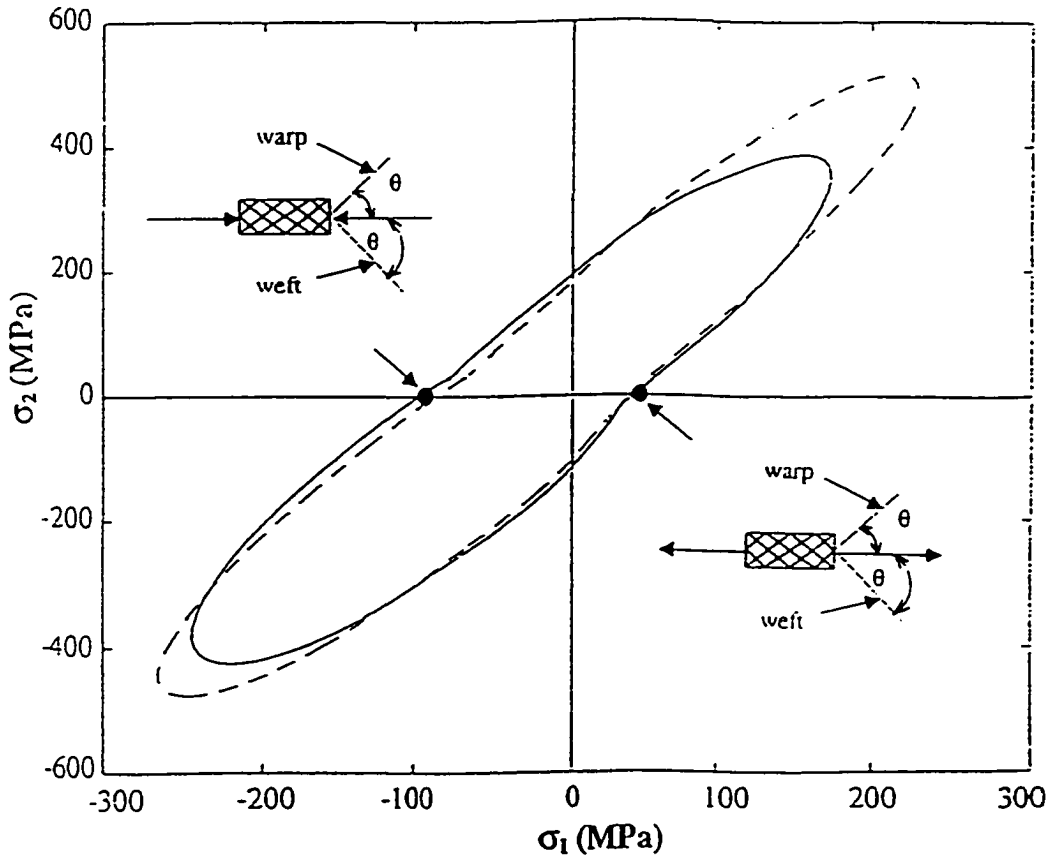

Figure 5.30 : In-plane ultimate strength envelopes of deformed plain-weave composite with $\theta = 57^0$ ($\sigma_{16} = 0$)

— Quadratic criterion using ply properties from measurement on fabric composite;

--- Quadratic criterion using ply properties from unidirectional composite;

● Experimental data.

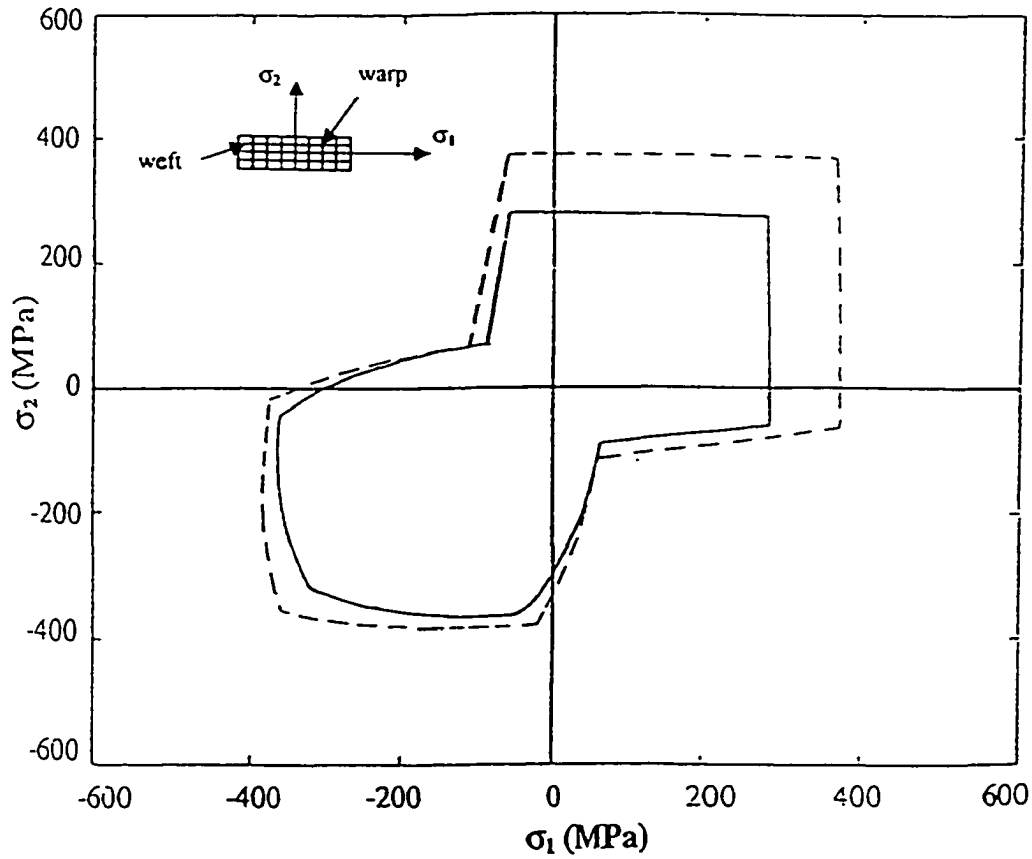

Figure 5.31 : In-plane ultimate strength envelopes for orthogonal plain-weave composite ($\sigma_{16} = 0$)

— Quadratic criterion using ply properties from measurement on fabric composite;

--- Quadratic criterion using ply properties from unidirectional composite;

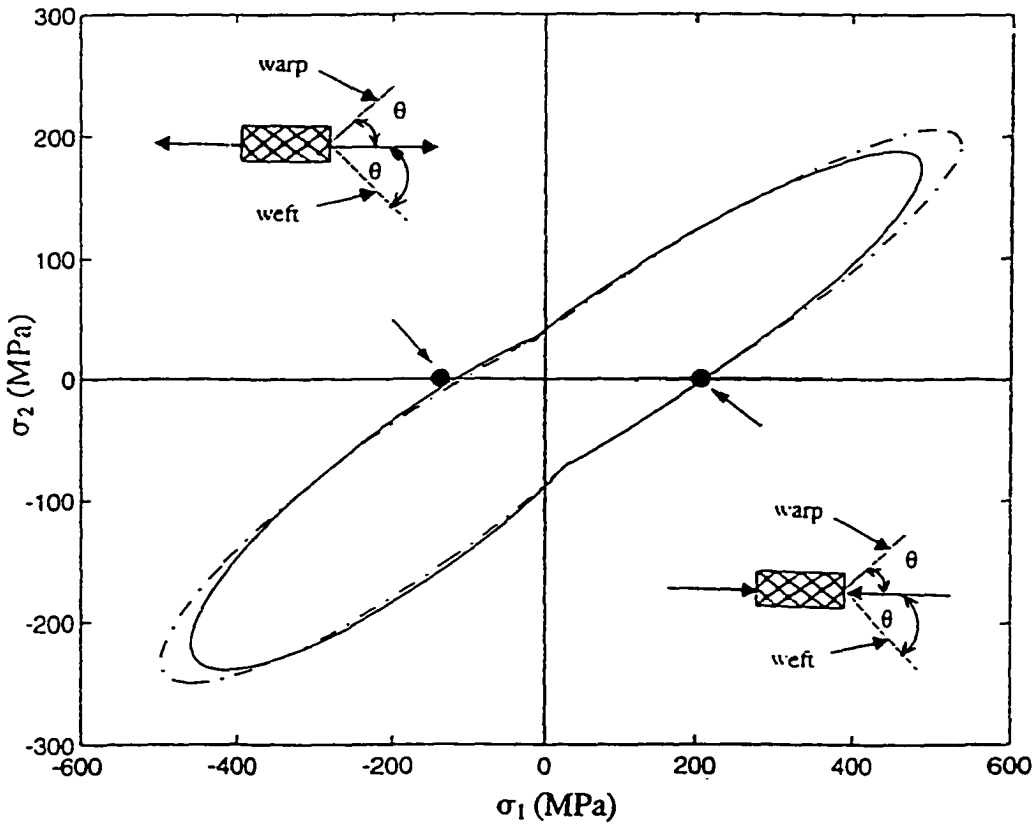

Figure 5.32 : In-plane ultimate strength envelopes of deformed 8-harness satin composite with $\theta = 31^0$ ($\sigma_{16} = 0$)

— Quadratic criterion using ply properties from measurement on fabric composite;

--- Quadratic criterion using ply properties from unidirectional composite;

● Experimental data.

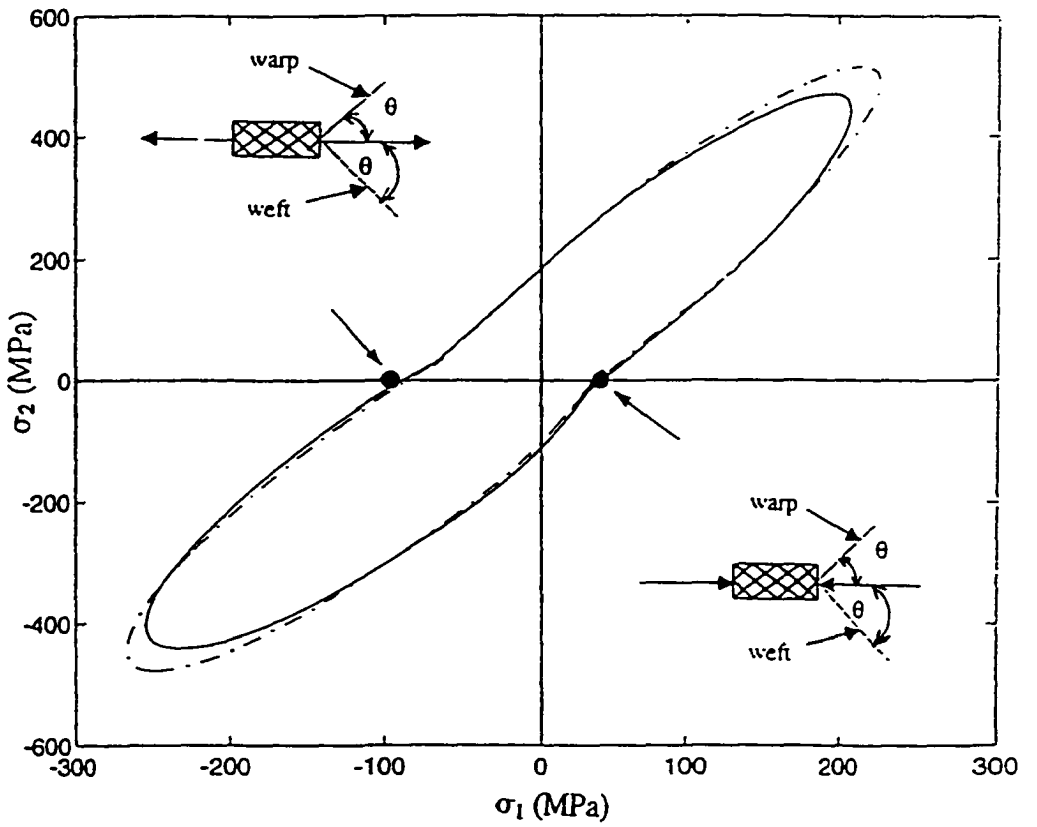

Figure 5.33 : In-plane ultimate strength envelopes of deformed 8-harness satin composite with $\theta = 57^0$ ($\sigma_{16} = 0$)

— Quadratic criterion using ply properties from measurement on fabric composite;

--- Quadratic criterion using ply properties from unidirectional composite;

● Experimental data.

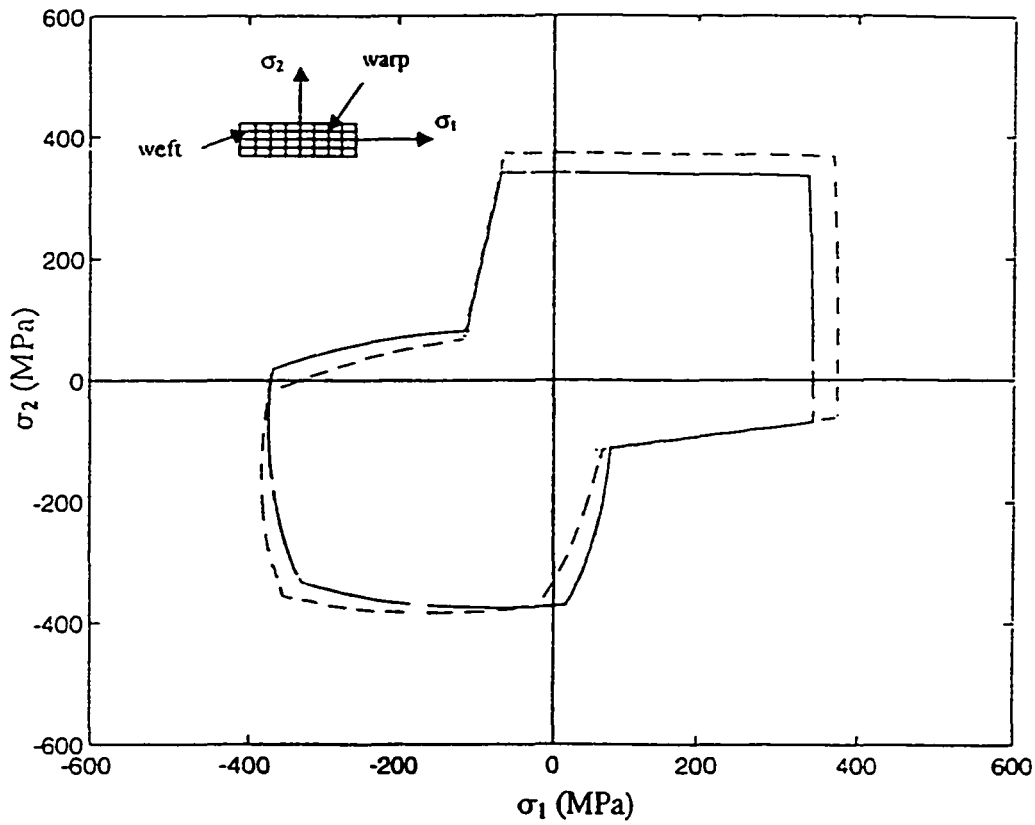

Figure 5.34 : In-plane ultimate strength envelopes for orthogonal 8-harness satin composite ($\sigma_{16} = 0$)

— Quadratic criterion using ply properties from measurement on fabric composite;

--- Quadratic criterion using ply properties from unidirectional composite;

Chapter 6

SUMMARY AND CONCLUSIONS

Strain at fracture varies as a function of the in-plane shearing deformation angle. In tensile test, strain at fracture at $\theta = 45^{\circ}$ reaches a maximum value, in the other hand, in compressive test, it is no longer maximum.

The damage development of woven fabric composite under tensile loading condition indicated that the damage was controlled by local state of stress and the region of damage zone can be expressed as a function of the in-plane shearing deformation angle.

We can see that failure modes of woven fabric composite is rather the same as one of laminated composites made of unidirectional plies. The sub-plies model again was proved that modelling woven fabric as a manner of laminated composite is completely reasonable.

The failure analysis and strength prediction of any deformed woven fabric laminates can be predicted by the sub-plies model. The results of the prediction are in good agreement with the experimental data. The fiber undulation has a strong effect on both transverse cracking and ultimate failure. The effect of fiber undulation can be taken into account by calculating the on-axis strength coefficients of the fictional constituent sub-plies directly on the samples made of woven fabric composites especially in the case of plain weave fabric.

REFERENCES

1. Adams, Donald F. 1992. "Test Methods for Composite Materials-Seminar Notes", Technomic Publishing Company, Lancaster, Pennsylvania .

2. Ashkenazi, E. K. 1966. "Problem of the Anisotropy of Strength", *Polymer Mechanics*, 1 : 69-72.

3. Assa, R. and Zvi, H. 1975. "Failure Modes of Angle Ply Laminates", *Journal of Composite Materials*, 9 : 191-206.

4. Azzi, V. D. and Tsai, S. W. 1965. "Anisotropic Strength of Composites", *Experimental Mechanics*, 5 : 283-288.

5. Carl, T. H. 1982. "Influence of Layer Thickness on The Strength of Angle-Ply Laminates", *Journal of Composite materials*, 16 : 216-227.

6. Chamis, C.C. and Sinclaire, J.H. 1977. "Ten-Degree Off-Axis Test for Shear Properties in Fiber Composites", *Experimental Mechanics*, 17 : 339-346.

7. Chou, T. W. and Ishikawa, T. 1989. "Analysis and Modeling of Two Dimensional Fabric Composites", In Textile Structural Composites. *Composites Materials Series*, T. W. Chou and F.Kko., R.B. Pipes, Series Ed.. Elsevier, NewYork, 3 : 209-264.

8. Chou, T.-W. 1985. "Strength and Failure Behavior of Textile Structural Composites", *First Conference on Composite Materials*, A.S.C., 1 : 104-116.

9. Davies, C. M. A., Harris, B. and Cooke, R. G. 1993. "Characterization of Damage Onset in Glass-Ceramic Matrix Composite Angle-Ply Laminates", *Composites*, 54 (2) : 141-149.

10. Ebeling, T., Hiltner, A. and Baer, E. 1997. "Delamination Failure of a Woven Glass Fiber Composite", *Journal of Composite Materials*, 31 : 1318-1333.

11. Elkin, M. A. 1984. "Mechanical Characterization and Failure Modes of Fiber Reinforced Angle Ply Composites", A Thesis Submitted to the Graduate Faculty of North Carolina State University at Raleigh – University Microfilms International.

12. Fisher, L. 1967. "Optimization of Orthotropic Laminates", *Journal of Engineering for Industry*, 89 : 399-402.

13. Franklin, H. G. 1968. "Classic Theories of Failure of Anisotropic Materials", *Fibre Science and Technology*, 1 : 137-150.

14. Ganesh, V. K. and Naik, N. K. 1997. "(±45) Degree Off-Axis Tension Test for Shear Characterization of Plain Weave Fabric Composites", *Journal of Composites Technology and Research*, JCTERE, 19 : 77-84.

15. Gol'denblat, I. and Kopnov, V. A. 1966. "Strength of Glass-Reinforced Plastics in the Complex Stress State", *Polymer Mechanics*, 1 : 54-59.

16. Hashin, Z. and Rotem, A. 1973. "A Fatigue Failure Criterion for Fiber Reinforced Materials", *Journal of Composite Materials*, 7 : 448-464.

17. Hill, R. 1948. "A Theory of the Yielding and Plastic Flow of Anisotropic Metals", *Proceeding of the Royal Society of London*, A193 : 282-287.

18. Hoffman, O. 1967. "The Brittle Strength of Orthotropic Materials", *Journal of Composite Materials*, 1 : 200-206.

19. Ishikawa, T. 1981. "Anti-Symmetric Elastic Properties of Composite Plates of Satin Weave Cloth", *Fiber Science & Techology*, 15 : 127-144.

20. Ishikawa, T. and Chou, T. W. 1982. "Stiffness and Strength Properties of Woven Composites", *Proceeding of the 4th International Conference on Composite Materials*, 4 : 489-496.

21. Ishikawa, T. and Chou, T.-W. 1982. "Elastic Behavior of Woven Hybrid Composites", *Journal of Composite Materials*, 16 : 2-19.

22. Ishikawa, T. and Chou, T.-W. 1982. "Stiffness and Strength Behavior of Woven Fabric Composites", *Journal of Material Science*, 17 : 3211-3220.

23. James, M. W., Issac, M. D. and Pipes R. B. 1982. "Experimental Mechanics of Fibre Reinforced Composite Materials", Published by the Society for Experimental Stress Analysis, Brookfield Center, Connecticut .

24. Jones, R. M. 1975. "Mechanics of Composite Materials", McGraw-Hill Book Company, NewYork.

25. Karayaka, M. and Kurath, P. 1994. "Deformation and Failure Behavior of Woven Composite Laminates", *Journal of Engineering Materials and Technology*, 116 : 222-232.

26. Kim, K. S. and Hong, C. S. 1986. "Delamination Growth in Angle-ply Laminated Composites", *Journal of Composite Materials*, 20 : 423-438.

27. Kim, R. Y. 1981. "On the Off-Axis and Angle-Ply Strength of Composite", *Test Methods and Design Allowable for Fibrous Composites*, ASTM STP 734, C. C. Chanis, Ed. , American Society for Testing and Materials, pp. 91-108.

28. Laroche, D. and Vu-Khanh T. 1993. "Modeling of the Thermo-Elastic Properties of Woven Fabric Composites in Complex Shapes", *Composite Materials : Testing and Design*, ASTM STP 1206, pp. 386-414.

29. Laroche, D.and Vu-Khanh T. 1992. "Modeling of the Forming of Complex Parts from Fabric Composites", *In Development and Design with Advanced Materials*, S.V. Hoa (Ed.), Elsevier Science Publishers B.V., North Holland, pp. 223-262.

30. Leif A. Carlsson and Byron Pipes, R. 1987. "Experimental Characterization of Advanced composite Materials", Prentice-Hall, Inc. – A Division of Simon and Schuster Englewood Cliffs, New Jersey.

31. Marin, J. 1957. "Theories of Strength for Combined Stresses and Non-isotropic Materials", *Journal of the Aeronautical Sciences*, 24 : 265-268.

32. Mark, J. S. 1989. "A Analysis of Shear Failure Mechanisms for Compression-Loaded $[\pm\theta]_s$ Laminates", *Journal of Composite Materials*, 23 : 251-263.

33. Nahas, M. N. 1986. "Survey of Failure and Post-Failure Theories of Laminated Fiber-Reinforced Composites", *Journal of Composites Technology and Research*, 8 : 138-153.

34. Naik, N. K. 1993. "Woven Fabric Composites", Technomic Publishing Company, Lancaster, Pennsylvania .

35. Naik, N. K. and Ganesh, V. K. 1991. "Micromechanical Analysis of Woven Fabric laminates", *Aerospace Engineering Department Indian Institute of technology*, Bombay-400 076.

36. Naik, N. K. and Ganesh, V. K. 1993. "Failure Behavior of Plain Weave Fabric Laminates under On-Axis Uniaxial Tensile Loading : III-Effect of Fabric Geometry", *Journal of Composite Materials*, 30 : 1823-1856

37. Naik, N. K., Shembekar, P. S. and Hosur, M. V. 1991, "Failure Behavior of Woven Fabric Composites", *Journal of Composites Technology and Research*, 13 : 107-116.

38. Norris, C. B. 1939. "The Elastic Theory of Wood Failure", ASME Transactions, 61 : 259-261.

39. Ohira, H. and Uda, N. 1985. "Knee Point and Post-Failure Behavior of Some Laminated Composites Subjected to Uniaxial Tension", *In Recent Advances in Composites in the United States and Japan*, ASTM STP 864, J. R. Vinson and M. Taya, Eds., American Society for Testing and Materials, Philadelphia, pp. 110-127.

40. Petit, P. H. and Waddoups, M. E. 1969. "A Method of Predicting the Nonlinear Behavior of Laminated Composites", *Journal of Composite materials*, 3 : 2-20.

41. Pipes, R.B. and Cole, B.W. 1973. "On the Off-Axis Strength Test for Anisotropic Materials", *Journal of Composite Materials*, 7: 246-256.

42. Puck, A. and Schneider, W. 1969. "On Failure Mechanisms and Failure Criteria of Filament-wound Glass Fibre Resin composites", *Plastics and Polymers*, 37 : 33-44.

43. Reifsnider, K. L. and Mirzadeh, F. 1988. "Compressive Strength and Mode of Failure of 8H celion300/PMR 15 Woven Composite Materials", *Journal of Composites Technology and Research*, 10 : 156-164.

44. Suhling, J. C., Rolands, R. E., Johnson, M. W. and Gunderson, D. E. "Tensorial Strength Analysis of Paperboard", *Experimental Mechanics*, 25 : 75-84.

45. Tsai, S. W. and Azzi V. D. 1966. "Strength of Laminated Composite Materials", *AIAA journal*, 4 : 296-301.

46. Tsai, S. W. and Haln, H. T. 1980. "Introduction to Composite Materials", Technomic Publishing Company, Inc. Lancaster, Pennsylvania.

47. Tsai, S.W. 1988. "Composites Design", Fourth edition, Think Composites, Dayton, Ohio.

48. Vu Khanh T. 1987. "Survey of Current Status and Future Trends in Reinforced Plastics Composites", Polymer Composites, 8 : 363-370.

49. Vu-Khanh T. and Nguyen-Hoa H. 1998. "Prediction of Failure in Unsaturated Polyester Reinforced by Plain Weave Glass Composite", *Proceedings of The Second Joint Canada-Japan Workshop on Composites*, pp.224-231.

50. Vu-Khanh T., Liu B. 1994. "Thermo-Elastic Behavior of Deformed Woven Fabric Composites at Elevated Temperature", Part I, *Proc. 9th Conf. American Society for Composites*, Dayton, OH, USA Sept., pp. 20-22.

51. Vu-Khanh T., Liu B. 1995. "Prediction of Fiber Rearrangement and Thermal Expansion Behavior of Deformed Woven Fabric Laminates", *Composite Science & Technology*, 53 : 183-191.

52. Vu-Khanh T., Liu B. 1997. "Characterization of Thermo-Elastic Behavior of Deformed Woven Fabric Composites at Elevated Temperatures", *Science & Engineering of Composite Materials*, 6 : 51-62.

53. Wang H., Vu-Khanh T. 1994. "Damage Extension in Carbon Fiber/PEEK Crossply Laminates under Low Velocity Impact", *Journal of Composite Materials*, 28 : 684-707.

54. Wu, E. M. 1974. "Phenomenological Anisotropic Failure Criterion", *Composite Materials*, Mechanics of Composite Materials, Academic Press, New York.

55. Wu, E. M. and Scheublein, J. K. 1974. "Laminate Strength : A Direct Characterization Procedure", *Composite Materials : Testing and Design*, ASTM STP546, pp. 188-206.